

**AN AUTOMATED APPROACH FOR THE MORPHOLOGICAL  
CHARACTERIZATION OF ACTIVATED SLUDGE FLOCS AND  
FILAMENTS USING IMAGE ANALYSIS**

By

**LEE XUE YONG**

A dissertation submitted to the Department of Electronic Engineering,  
Faculty of Engineering and Green Technology,  
Universiti Tunku Abdul Rahman,  
in partial fulfillment of the requirements for the degree of  
Master of Engineering Science  
August 2015

## **ABSTRACT**

### **AN AUTOMATED APPROACH FOR THE MORPHOLOGICAL CHARACTERIZATION OF ACTIVATED SLUDGE FLOCS AND FILAMENTS USING IMAGE ANALYSIS**

**Lee Xue Yong**

Activated sludge process is commonly used for purification of wastewater. The proper settling of the sludge flocs in the activated sludge wastewater treatment process is crucial to the normal functioning of the system, where sludge bulking/filamentous bulking presents a common and persistent problem that prevents good floc settleability. As a new form of technology, image processing and analysis methods present potential solutions to the long standing problem of filamentous bulking faced by activated sludge wastewater treatment plants around the world in a fast and timely manner. The main objects of interest under microscopic inspections are the sludge flocs and the filamentous organisms. In this research, illumination-invariant algorithms to segment the floc and the filament objects in the microscopic sludge images captured at 40 times and 100 times total magnification in brightfield microscopy have been developed. Analyses of the morphological parameters of the segmented objects are also done. The standard physico-chemical tests of SVI, MLSS as well as laser particle sizing for the sludge samples are conducted simultaneously with image acquisition and the results of both methods are compared with each other to investigate the

effectiveness of digital image processing and analysis to act as a monitoring system in the activated sludge wastewater treatment process. Average accuracies of 71.85% and 67.86% respectively in Dice coefficient values have been calculated from the image samples processed with the floc segmentation algorithm and filament segmentation algorithm. It has been found that the results from digital imaging methods correlate well with those from non-imaging methods by means of similar shape of graph lines plotted from different methods. For similarity of graph line shape, Pearson's correlation coefficient returns values larger than 0.8 in 5 of 6 samples processed for comparing the method of digital imaging and laser particle sizing. Morphological analyses of the floc objects have also found a significant correlation pattern between the results obtained and the results from SVI (Sludge Volume Index). Study in required images for processing suggests 20 images as sufficient for processing flocs.

## **ACKNOWLEDGEMENTS**

My sincere gratitude to supervisor and co-supervisor Dr. Humaira Nisar and Dr. Yeap Kim Ho for all the patience and kindness that I have received to have managed to let me complete my master degree's research work. And also to Dr. Ng Choon Aun for the guidance and cooperation that I have received during the time of research advising me in my work.

Without the help and effort of co-researcher and friend Muhammad Burhan Khan the image acquisition work would not have been possible. My best wishes for him for his progress in obtaining his PhD. degree.

## APPROVAL SHEET

This dissertation/thesis entitled “**AN AUTOMATED APPROACH FOR THE MORPHOLOGICAL CHARACTERIZATION OF ACTIVATED SLUDGE FLOCS AND FILAMENTS USING IMAGE ANALYSIS**” was prepared by LEE XUE YONG and submitted as partial fulfillment of the requirements for the degree of Master of Engineering Science at Universiti Tunku Abdul Rahman.

Approved by:

---

(Prof. Dr. \_\_\_\_\_ )

Date:.....

Professor/Supervisor

Department of Electronic Engineering

Faculty of Engineering and Green Technology

Universiti Tunku Abdul Rahman

---

(Prof. Dr. \_\_\_\_\_ )

Date:.....

Professor/Co-supervisor

Department of Engineering

Faculty of Engineering and Green Technology

Universiti Tunku Abdul Rahman

**FACULTY OF ENGINEERING AND GREEN TECHNOLOGY**

**UNIVERSITI TUNKU ABDUL RAHMAN**

Date: \_\_\_\_\_

**SUBMISSION OF FINAL YEAR PROJECT /DISSERTATION/THESIS**

It is hereby certified that Lee Xue Yong (ID No: 12AGM06075 ) has completed this final year project/ dissertation/ thesis\* entitled "An automated approach for the morphological characterization of activated sludge flocs and filaments using image analysis" under the supervision of Dr. Humaira Nisar (Supervisor) from the Department of Electronic Engineering, Faculty of Engineering and Green Technology, and Dr. Yeap Kim Ho (Co-Supervisor)\* from the Department of Electronic Engineering, Faculty of Engineering and Green Technology.

I understand that University will upload softcopy of my final year project / dissertation/ thesis\* in pdf format into UTAR Institutional Repository, which may be made accessible to UTAR community and public.

Yours truly,

\_\_\_\_\_

## DECLARATION

I hereby declare that the dissertation is based on my original work except for quotations and citations which have been duly acknowledged. I also declare that it has not been previously or concurrently submitted for any other degree at UTAR or other institutions.

Name \_\_\_\_\_

Date \_\_\_\_\_



## TABLE OF CONTENTS

	<b>Page</b>
<b>TITLE PAGE</b>	<b>i</b>
<b>ABSTRACT</b>	<b>iii</b>
<b>ACKNOWLEDGEMENTS</b>	<b>v</b>
<b>APPROVAL SHEET</b>	<b>vi</b>
<b>SUBMISSION SHEET</b>	<b>vii</b>
<b>DECLARATION</b>	<b>viii</b>
<b>TABLE OF CONTENTS</b>	<b>ix</b>
<b>LIST OF TABLES</b>	<b>xi</b>
<b>LIST OF FIGURES</b>	<b>xii</b>
<b>CHAPTER</b>	
<b>1.0 INTRODUCTION</b>	<b>1</b>
1.1 Motivation of Study	1
1.2 Fundamentals of Digital Image, Digital Image Processing and Analysis	2
1.3 Wastewater Treatment Process	4
1.3.1 The Activated Sludge Wastewater Treatment System	7
1.3.1.1 Filamentous Bulking as an Abnormal Condition	10
1.3.1.2 Standard Conventional Monitoring Methods and Definitions	13
1.3.1.3 Laser Particle Sizing Method	15
1.4 Research	16
1.4.1 Problem Statement	16
1.4.2 Objectives	17
1.4.3 Organisation of Dissertation	17
<b>2.0 LITERATURE REVIEW</b>	<b>19</b>
2.1 Effectiveness of Image Analysis Methods	19
2.2 Image Acquisition and Image Analysis	22
<b>3.0 MATERIALS AND METHODS</b>	<b>31</b>
3.1 Methodology Overview	31
3.2 Image Acquisition	32
3.3 Physico-Chemical Tests	34
3.4 Floc Segmentation Algorithm	35

3.4.1	Stepwise Flow	35
3.4.2	Explanations and Elaborations	37
3.5	Filament Segmentation Algorithm	39
3.5.1	Stepwise Flow	39
3.3.2	Explanations and Elaborations	42
3.6	Assessment of Segmentation Accuracy	48
3.7	Morphological Parameters for Analysis of Floes	49
<b>4.0</b>	<b>RESULTS AND DISCUSSIONS</b>	<b>50</b>
4.1	Step by Step Output Images	50
4.1.1	Floc Segmentation Algorithm	50
4.1.2	Filament Segmentation Algorithm	52
4.2	Ground Truth Floc Segmentation Accuracy Test	57
4.3	Ground Truth Filament Segmentation Accuracy Test	63
4.4	Assessment via Comparisons with non-Digital Imaging Methods	68
4.5	Floc Object Morphological Parameter Analysis	76
4.6	Study on the Appropriate Number of Images for Processing	83
<b>5.0</b>	<b>CONCLUSIONS AND FUTURE DIRECTIONS</b>	<b>86</b>
5.1	Overview	86
5.2	Future Work Recommendations	87
	<b>REFERENCES</b>	<b>88</b>
<b>APPENDIX A</b>	Matlab Programming Code	<b>95</b>

## LIST OF TABLES

<b>Table</b>		<b>Page</b>
1.1	SVI Values and Conditions	14
2.1	Literature Review	24
4.1	Dice Coefficient Values for Floc Images	63
4.2	Dice Coefficient Values for Filament Images	68
4.3	Sludge Volume Index and Total Suspended Solids	74
4.4	Pearson Correlation Coefficients for Sample 1 to Sample 6	78
4.5	Average Values of Morphological Parameters for Floc Objects Divided into Three Size Classes for Sample 1 to Sample 6	79
4.6	Average Values of Morphological Parameters for Size-Undivided Floc Objects for Sample 1 to Sample 6	81

## LIST OF FIGURES

<b>Figures</b>	<b>Page</b>
1.1 Digital Image Concept Illustration	2
1.2 Generalized Wastewater Treatment Diagram	5
1.3 Conventional Activated Sludge Wastewater Treatment Flow Diagram	9
1.4 Floc Settlement	11
1.5 Filamentous Bulking	11
1.6 Good Quality Mixed Liquor	12
1.7 Laser Particle Sizing Method	15
2.1 Course of SVI Values for Two Tanks	20
2.2 Microscopic Picture of an Activated Sludge Sample from Aeration Tank 1 at Day 7	21
2.3 Microscopic Picture of an Activated Sludge Sample from Aeration Tank 2 at Day 7	21
3.1 Flowchart of Methodology	32
3.2 Sample 'Floc' Image with x4 Objective Magnification	33
3.3 Sample 'filament' image with x10 objective magnification	34
3.4 Flowchart of Floc Segmentation Algorithm	36
3.5 Flowchart of Filament Segmentation Algorithm	41
4.1 Steps of Floc Segmentation Algorithm	51
4.2 Steps of Filament Segmentation Algorithm	53
4.3 Assessment of Floc Segmentation	58

4.4	Assessment of Filament Segmentation	64
4.5	Floc Volume Percentage vs Particle Size Distribution Graphs for 6 Samples for Digital Imaging and Laser Particle Size Analyser Methods	69
4.6	Floc Volume Percentage vs Particle Size Distribution Graphs for 8 Samples for Digital Imaging and Laser Particle Size Analyser Methods	70
4.7	Line Graph for IA Using and IA & TSS Using Methods across 6 Days	75
4.8	Image with Floc Objects Segmented and Respective 'Roundness' Values Labelled	77
4.9	Chart of morphological parameter and SVI values for 6 samples	82
4.10	Chart of morphological parameter and SVI values for small objects for 6 samples	82
4.11	Chart of morphological parameter and SVI values for medium objects for 6 samples	83
4.12	Chart of morphological parameter and SVI values for large objects for 6 samples	83
4.13	Number of Images Processed vs The Mean Number of Floccs per Image Distribution Graph over 6 Samples	84

## **CHAPTER 1**

### **INTRODUCTION**

#### **1.1 Motivation of Study**

Activated sludge wastewater treatment plants are commonly used in large cities and communities worldwide for purification of wastewater. For the activated sludge process to be successful and to function normally, the proper settling of the sludge flocs in the activated sludge wastewater treatment process is an essential condition.

Preventing the normal functioning of the plants is to be found the common and persistent problem of sludge bulking/filamentous bulking. This abnormal condition involves the overgrowth of filamentous bacteria or filaments, causing the sludge flocs to be unable to settle/sediment properly due to structural disruptions and ultimately lowering the performance of the plants.

Under microscopic observations, different structural characteristics and quantity are observed for the floc objects and the filament objects of the activated sludge samples for different plant performance conditions. Structural changes occur even before changes in measurement data using the traditional physico-

chemical methods are detected. As such, image processing and analysis methods present potential solutions as an additional complementary monitoring system to the long standing problem faced by activated sludge wastewater treatment plants around the world; incompletely solved by traditional established methods. Abnormal conditions may also be predicted and remedied in time using digital imaging methods.

## 1.2 Fundamentals of Digital Image, Digital Image Processing and Analysis

An image can be defined as a two-dimensional signal, represented by a function  $f(x,y)$  where the function value represents intensity or colour information for a given point specified by the spatial coordinates  $x$  and  $y$ . When  $x$ ,  $y$ , and the amplitude values of  $f$  are all finite, discrete quantities, the image that is being represented is a digital image (Gonzalez et al., 2009). Otherwise, it is an analogue image. It is possible to specify the smallest displayable point for digital images due to their discrete nature. This point is known as a pixel.

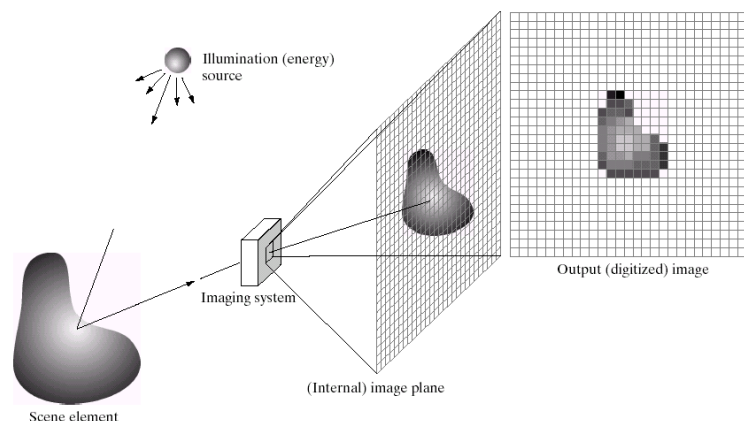


**Figure 1.1: Digital image concept illustration (Gonzalez et al., 2009)**

Digital image processing and analysis can be defined as processes whose inputs and outputs are digital images. They extract attributes from the images, and can recognize individual object based on these attributes.

Both image processing and image analysis have been simultaneously covered by using the above term. By the basis of their difference in output, one may describe image processing as any form of information processing which uses images as input data and produces transformed/modified images as output, and image analysis as any form of information processing that uses images as input data and produces descriptions and characteristics of them as output. Generally, all variations in definitions presume that image processing techniques are performed first, and then image analysis techniques are applied. However, there is no general consensus among authors regarding where image processing stops and the related areas, image analysis and computer vision begin (Gonzalez et al., 2009). Hence, in general literature usage, the terms “image processing” and “image analysis” are not strictly differentiated from each other; either term can usually be assumed to take on the definition of the wider comprehensive term.

Generally, images are modified and transformed via image processing techniques to improve their pictorial information for human interpretation, or to render them more suitable for autonomous machine perceptions (McAndrew, 2004). Humans like their images to be sharp, clear and detailed while machines prefer their images to be simple and uncluttered (McAndrew, 2004).



For human interpretation purposes, useful operations include edge enhancement, noise removal, and blur removal; for machine perception, edge detection and detail removal are helpful operations. At present, image processing is finding more and more uses in a wide variety of fields concerning many different operations. Image processing is done for multipurpose image enhancement/restoration, artistic effects, medical visualisation, industrial inspection, law enforcement, human computer interfaces, and other purposes and fields. In the biological sciences, the understanding of various features of cell biology, molecular biology and neuroscience among others all call for a critical part and role for visualizations and image processing and analysis methods to play in. Not only are structural characteristics visualized and studied, but they are also increasingly transformed into more quantitative data and measurements for further studies to be made upon them.

### **1.3 Wastewater Treatment Process**

According to the Food and Agriculture Organization of the United Nations, wastewater treatment generally has a principal objective of allowing human and industrial effluents to be disposed of without danger to human health or unacceptable damage to the natural environment. By combining physical, chemical, and biological processes and operations, solids, biodegradable organic

matter, pathogenic bacteria and sometimes nutrients are removed from wastewater in conventional wastewater treatment processes.

A generalized wastewater treatment diagram is seen in Figure 1.2.

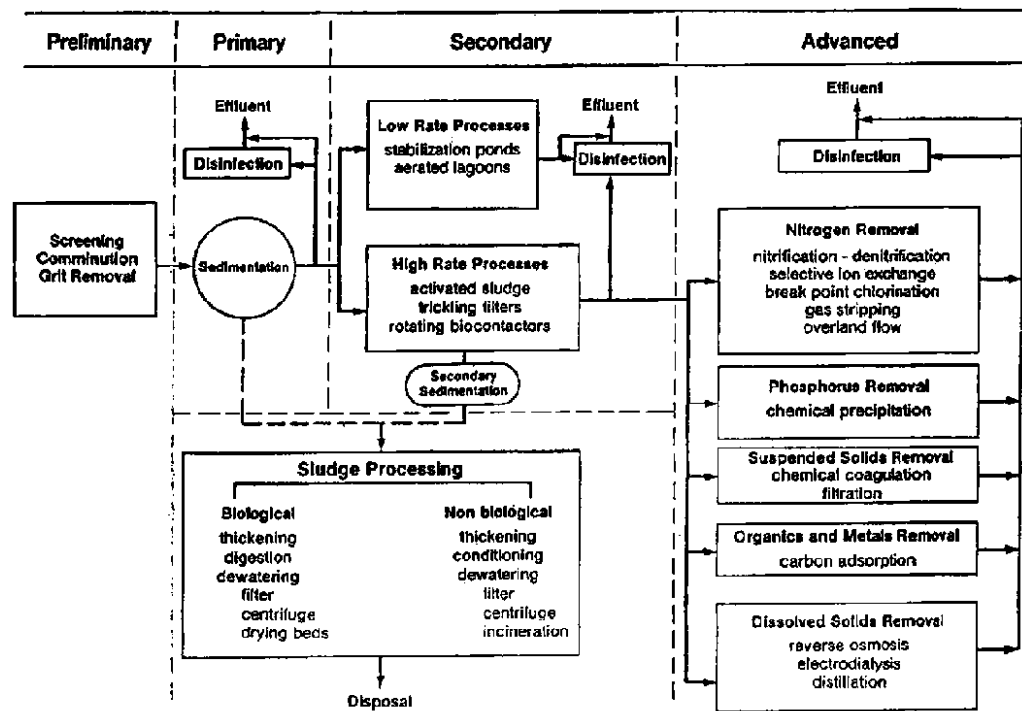


Figure 1.2: Generalized wastewater treatment diagram (Asano et al., 1985)

It can be seen from Figure 1.2 that there are at least three levels of wastewater treatment: primary, secondary, and tertiary or advanced. Additionally, there is a preliminary treatment process that is aimed at removing coarse solids and other large materials often found in raw wastewater.

Primary treatment process is also known as the mechanical treatment level. In this level both suspended and floating solids and settleable solids by sedimentation are separated and removed from raw sewage and the process itself is generally the first stage of wastewater treatment. The Food and Agriculture Organization of the United Nations (FAO) states that around 25 to 50% of the incoming biochemical oxygen demand (BOD<sub>5</sub>), 50 to 70% of the total suspended solids (SS), as well as 65% of the oil and grease are removed during primary treatment.

Primary treatment is followed by the secondary treatment stage which is considered a 'biological' stage compared to other stages. Microorganisms which feed on the residue waste and organic matter are employed and generally aerobic biological treatment processes are involved. Activated sludge, trickling filters, rotating biological contactors are all commonly used high-rate processes, defined by relatively small reactor volumes and high concentrations of microorganisms. Combined with primary treatment, the FAO states that a total of 85 % of the BOD<sub>5</sub> and SS originally present in the raw wastewater and some of the heavy metals are typically removed from the effluent.

Additional treatment beyond secondary stage is considered tertiary or advanced treatment. The stage is employed when specific wastewater constituents that the previous treatment process cannot remove must be removed. Tertiary

treatment is capable of removing more than 99 percent of all the impurities from wastewater to produce an effluent approaching drinking-water quality.

### **1.3.1 The Activated Sludge Wastewater Treatment System**

It can be seen from the previous section that the various terms for different methods of wastewater treatment mainly refer to the different method used in/for the secondary biological treatment stage. However, it can be safely assumed that when any wastewater treatment methods are mentioned, they refer to the entire wastewater treatment process flow encompassing all stages and not just the secondary stage.

The activated sludge process/ wastewater treatment process was invented in the 20<sup>th</sup> century around 1914 in England. It is considered to be the most widely used biological wastewater treatment process today due to its effectiveness and flexibility since its invention from approximately one century before.

The activated wastewater treatment process essentially involves:

1. The aeration of wastewater with aerobic microorganisms present
2. The removal of biological solids by means of sedimentation
3. The returning/recycling of settled biological solids back into the aerated wastewater

Point three is the single most important distinguishing feature of the activated sludge treatment process compared to other methods invented and in use before itself. Whenever wastewater is continuously aerated, enough oxygen is eventually dissolved in the affluent such that various aerobic bacteria and other types of microorganisms are able to grow, multiply, and consume the organic solids/pollutants present in the affluent as “food”, oxidizing organic matter in water to carbon dioxide and water (Bengtson and Malburg, 2011a). In the process, the biomass known as “sludge flocs” that would eventually settle is formed and the affluent becomes purified. However, without the recycling of the aerobic microorganisms to raise their concentration in the wastewater, the biological oxidation and purification is a very slow process (Bengston and Stonecypher, 2013).

By continually returning most of the sludge flocs or the “activated sludge” formed at the later stage in suitable amounts to the wastewater at the beginning, the new system’s purification performance is improved (Tchobanoglous et al., 2002; Grady et al., 1999; Vesilind et al., 2004).

The activated sludge process has the advantage of producing a high quality effluent at reasonable operating and maintenance costs. Activated sludge wastewater treatment plants are widely used all around the world in large cities and communities where large volumes of wastewater must be highly treated

economically. A diagram of a conventional activated sludge wastewater treatment plant is shown in Figure 1.3.

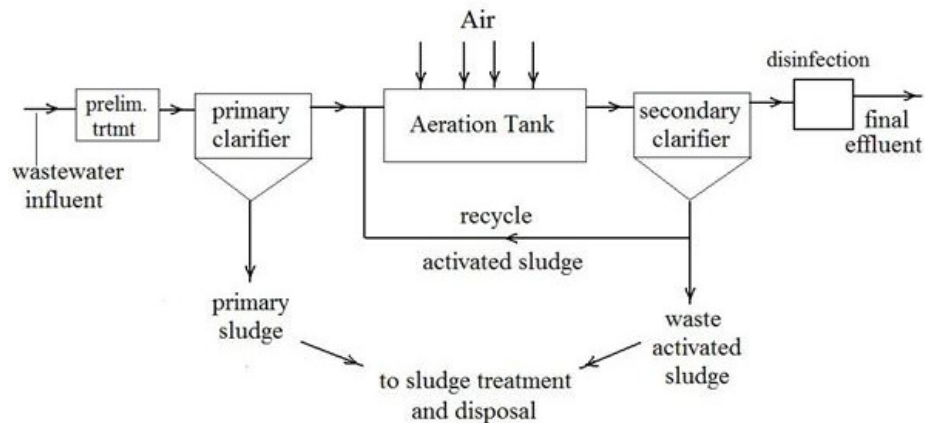


**Figure 1.3: Conventional activated sludge wastewater treatment flow diagram**

(Credit: <http://www.brighthub.com/environment/science-environmental/articles/66158.aspx> )

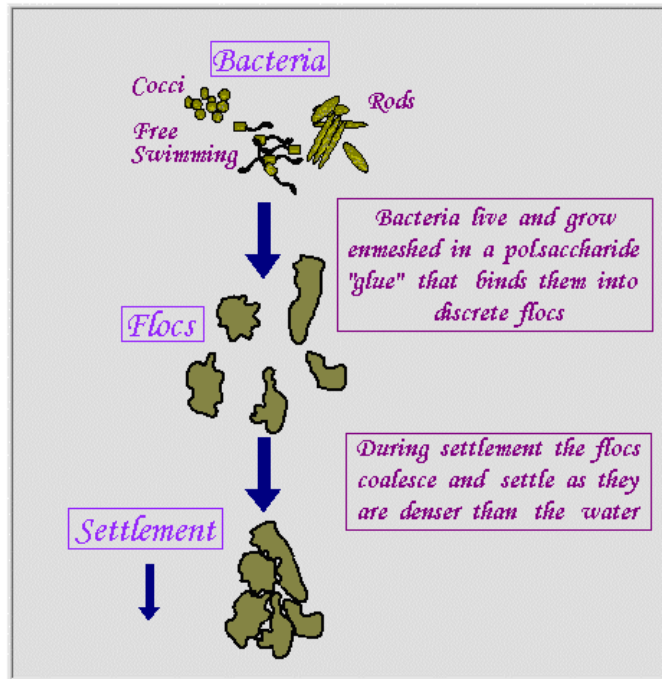
Variations in activated sludge wastewater treatment systems exist in addition to the conventional variety depicted in Figure 1.3 (Bengtson and Malburg, 2011b). In all of the varieties, the secondary clarifier and the aeration tank/basin are present. The secondary clarifier serves as the place where the sludge flocs that have been formed are supposed to coalesce and settle to become the activated sludge. The term mixed liquor is used to refer to the combination of the wastewater influent and the return activated sludge.

In the secondary clarifier of an activated sludge wastewater treatment plant, the sludge flocs of the mixed liquor within must coalesce and settle properly so that the resultant activated sludge is produced, and also for them to not get carried

over to the next procedure as treated effluents to negatively reduce the effluent's quality.

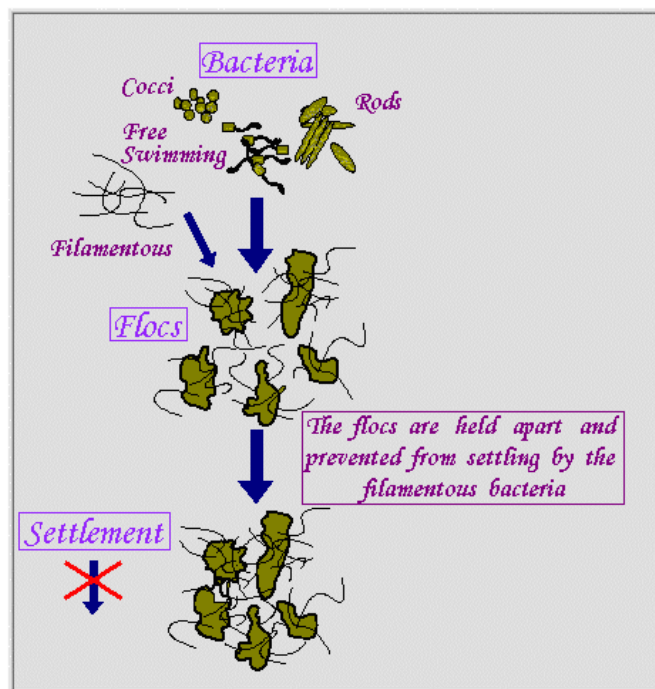
#### **1.3.1.1 Filamentous Bulking as an Abnormal Condition**

Figure 1.4 illustrates the processes in a good quality mixed liquor where the flocs compact and coalesce and proper floc settlement occurs. Figure 1.5 illustrates a case of filamentous bulking; here, the mixed liquor involved would be slow and difficult in sedimentation due to the observed disturbances by the filamentous microorganisms. As can be seen from Figure 1.5, the proper “gluing/binding together” of the flocs have been effectively hindered by the growth of the filaments that is excessive. As such, the effluent becomes polluted with the flocs that do not bind together and do not settle.



**Figure 1.4: Floc settlement**

(Credit: <http://web.deu.edu.tr/atiksu/ana52/ani4091.html> )



**Figure 1.5: Filamentous bulking**

(Credit: <http://web.deu.edu.tr/atiksu/ana52/ani4091.html> )



The characteristics of good quality mixed liquor can be seen in Figure 1.6. Under microscopic observations, the most relevant characteristics would be the strong, large flocs indicating a balance between floc formers and filament forming bacteria.

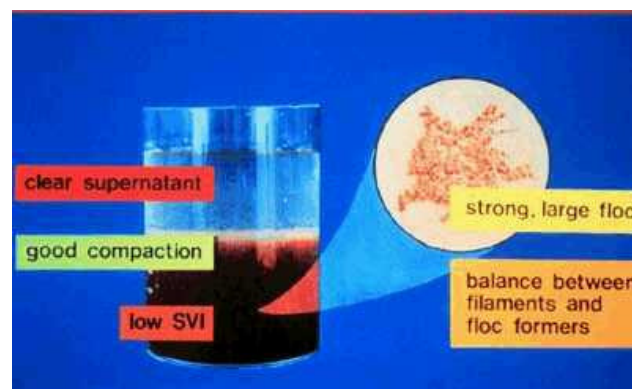


**Figure 1.6: Good quality mixed liquor**  
(Credit: <http://web.deu.edu.tr/atiksu/ana52/ani4091.html> )

Filamentous bulking/ bulking sludge is a common and persistent problem that has affected all activated sludge wastewater treatment plants since the early days of the process's invention and treatment use. Low oxygen concentration, low food to mass (F/M) ratio, wastewater septicity, low nutrient conditions are all among the causes for filament overgrowth, preventing good mixed-liquor solid compaction and settlement. In the monitoring of wastewater treatment plants' performances using image analysis techniques against filamentous bulking and as a whole, the monitoring of filamentous microorganism/filament growth plays an important part.

### 1.3.1.2 Standard Conventional Monitoring Methods and Definitions

There are various physico-chemical methods that are used traditionally to monitor the performance of the activated sludge wastewater treatment plants. The most important ones and those most relevant to our study are discussed below.

- Mixed Liquor Suspended Solids (MLSS): Total suspended solids (TSS) in the aeration tank of the wastewater treatment plant is termed as MLSS.
- Mixed Liquor Volatile Suspended Solids (MLVSS): Volatile suspended solids (VSS) in the aeration tank of the wastewater treatment plant is called MLVSS.
- Sludge Volume Index (SVI): Sludge volume index is defined as the volume in mL occupied by 1gram (g) of activated sludge preceded by settling of the mixed liquor for 30 minutes. It is determined by using the following formula:

$$SVI = \frac{SSV30 \times 1000}{MLSS} \text{ (mL/g)} \quad (1.1)$$

where SSV30 is the volume of settled sludge in Imhoff cone containing 1 Litre (L) sample of mixed liquor noted after 30 minute.

MLSS is defined by the following formula:

$$MLSS = \frac{(A - B) \times 1000}{\text{Volume of mixed liquor sample in Litres}} \text{ (mg/L)} \quad (1.2)$$

where A is the weight of the filter plus dried sample residue in milligrams (g) and B is the weight of the filter only in mg.

Generally speaking, relatively low SVI values indicate good settling ability for the sludge although values that are too low may point towards another type of abnormal condition, namely the pinpoint floc condition. A value of lower than 120 mL/g may be considered satisfactory while a value greater than 150 mL/g indicates a bulking condition for the sludge and the plant (Jenkins et al., 2003). However, all SVI values and indicated condition given are not fixed and may vary depending on different plant parameters. In Table 1.1 is shown some typical SVI values and conditions for reference.

**Table 1.1: SVI Values and Conditions**

SVI (ml/g)	Indicated Condition
< 50	Pinfloc Potential
50 to 100	Good Range
100 to 150	Filament Growth
150 to 200	Bulking at High Flows
200 to 300	Bulking
> 300	Severe Bulking

(Credit: <http://www.wrights-trainingsite.com/ActSlud1onb.html>)

### 1.3.1.3 Laser Particle Sizing Method

Laser particle sizing or laser particle size analysis method is a method that utilizes laser diffraction analysis to measure sizes of particles found within a sample. An illustration of the method is shown in Figure 1.7.

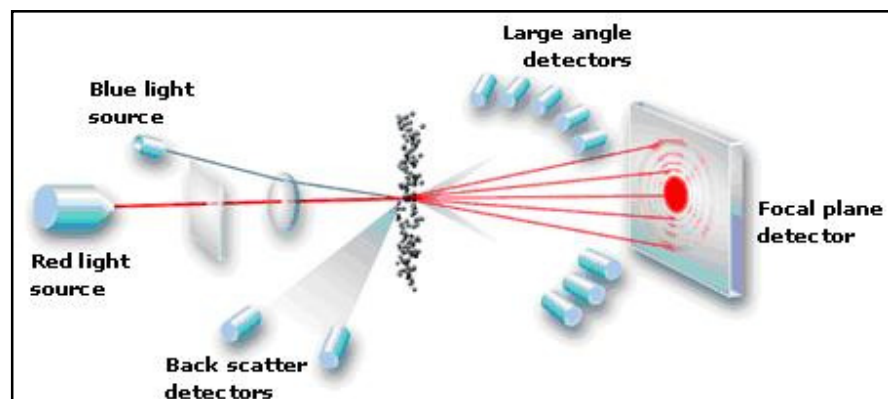


**Figure 1.7: Laser particle sizing method**

(Credit: <http://particle.dk/methods-analytical-laboratory/particle-size-by-laser-diffraction/laser-diffraction-theory/>)

In Figure 1.7, the blue light source is for measurements of small particles and the red one for the detection of larger particles. It is possible to measure particle sizes from the range of roughly 0.02 up to 2000  $\mu\text{m}$  and above depending on the lens used and then produce a particle size distribution graph from the measured data by using one from the two calculation models of Fraunhofer approximation or the Mie theory.

## **1.4 Research**

### **1.4.1 Problem Statement**

For the purpose of our study, it has been observed that:

- Changes in test measurements (SVI, etc) occurs with a delay, hence little or no time for precautionary measure is left once sedimentation problems take place (Gins et al., 2005).
- Changes in sludge floc morphology that reflect condition changes happen quicker and hence can tell state of plants beforehand if microscopic analyses can be done and correlated to physic-chemical test values.
- The laser particle analysis is also utilized to measure the sludge object's size distribution. The laser particle analyser however, is expensive and hence this is an uneconomical monitoring method.
- Available literatures do not clearly describe and assess segmentation techniques/algorithms used; Built in image analysis software methods are used in many instances.

### **1.4.2 Objectives**

The objectives of this research are as follow:

- ▶ To utilize digital image processing techniques to develop automated methods that identify the flocs and the filaments found in the activated-sludge wastewater treatment process.
- ▶ To quantify and morphologically analyse the flocs and the filaments identified.
- ▶ To correlate digital imaging methods in this work with the established physico-chemical methods.

### **1.4.3 Organisation of Dissertation**

The rest of the dissertation is organized as follows:

Chapter 2 provides literature review of image processing and analysis techniques used in activated sludge wastewater treatment systems.

Chapter 3 describes the materials and methods that have been utilized in the study. It gives an overview of sample collection and preparation under the overall process of image acquisition, and also describes the algorithms developed and the associated principles in steps.

Chapter 4 documents the result of the proposed algorithms. It includes assessment of proposed algorithms and correlation and morphological parameter analyses.

Finally the dissertation is concluded. This chapter concludes the dissertation and gives directions/recommendations for improvement and future studies.

The conclusion segment is followed by references. Credits for images used in this dissertation from various sources are included in this section.

## CHAPTER 2

### LITERATURE REVIEW

#### 2.1 Effectiveness of Image Analysis Methods

Conventional physico-chemical methods utilizing SVI (sludge volume index) tests and others are unable to detect filamentous bulking events in time to effectively remedy the abnormal situations (Gins et al., 2005). On the other hand, the ability of different image analysis methods to be used as activated sludge monitoring systems has been positively confirmed by many authors after comparisons with the classical physico-chemical methods (eg. SVI measurement) (Amaral et al., 1999; Heine et al., 2000; Heine et al., 2001; Da Motta et al., 2001a; Dagot et al., 2001; Amaral, 2003; Mesquita et al., 2008; Mesquita et al., 2010).

Yu et al. (2009) managed to obtain closely correlated results with activated sludge particle size measured by means of laser particle sizing method and the size obtained from image analysis method. In the work of Heine et al. (2000) and Heine et al. (2001), it is found that excessive growth of filamentous bacteria is recognisable by microscopic images of the activated sludge approximately 2 to 3 days earlier than by physical-chemical parameters. The



authors have built lab scale systems applying different controlled parameters and have compared results of SVI measurements with the image analysis results.

Figure 2.1 to Figure 2.3 show the results by the researchers.

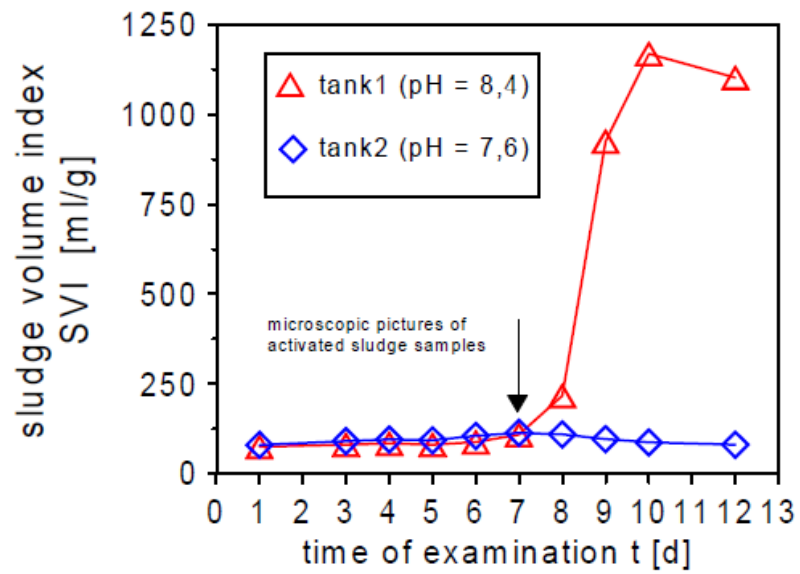


**Figure 2.1: Course of SVI values for two tanks (Heine et al., 2000)**

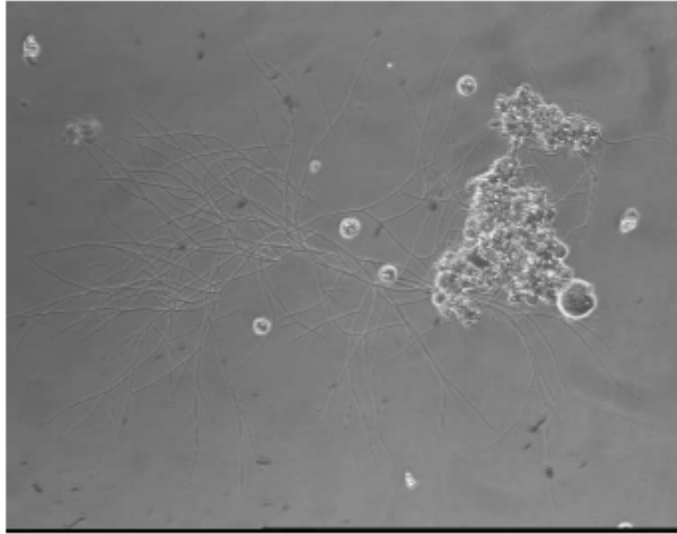


**Figure 2.2: Microscopic picture of an activated sludge sample from aeration tank 1 at day 7 (Heine et al., 2000)**

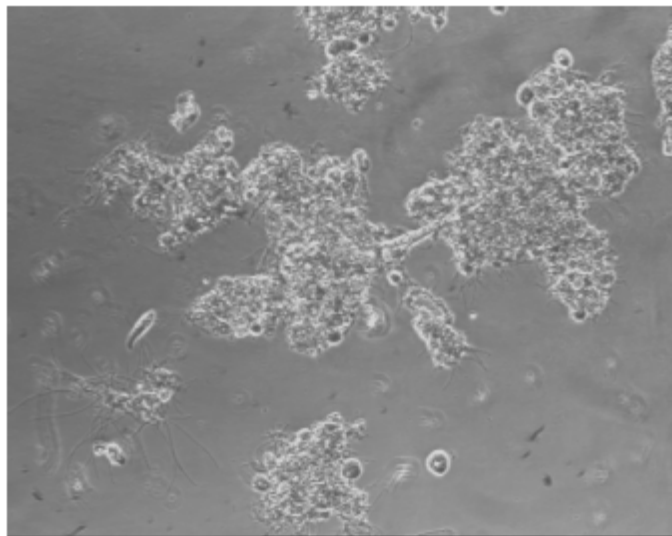


**Figure 2.3: Microscopic picture of an activated sludge sample from aeration tank 2 at day 7 (Heine et al., 2000)**

It can be seen in Figure 2.1 that while the sudden rise in the SVI value line in the graph happens at around day 8-9 with the dot of day 7 having a comparatively normal value, filament objects are already detected in the observed microscopic picture of the sludge at day 7.

## **2.2 Image Acquisition and Image Analysis**

For sludge floc microscopic image observations, there has been usage of high magnifications to observe bacterial compositions and filamentous bacteria inside the sludge. Usage of low magnifications (eg. 50× or 100×) to observe the flocs and the filaments combined with image analysis has since become more common (Liwarska-Bizukojc, 2005). The latter method is simpler in its image acquisition sample preparation being non-laborious and the results obtained are also more objective and reproducible due to the automated image analysis process employed (Liwarska-Bizukojc, 2005).

For the number of images required to obtain statistically relevant results, Liwarska-Bizukojc and Bizukojc (2005) reported to confirm that 40 is a sufficient number.

In the work of Amaral (2003), the author divided the aggregate objects of his study into 3 size classes in his aerobic wastewater treatment process research section. They have been divided into 3 size classes of aggregates ranging from having an equivalent diameter of 0.0184 mm up to 0.1 mm, aggregates ranging from having an equivalent diameter of 0.1 mm up to 1 mm, and finally aggregates with an equivalent diameter larger than 1 mm. The smallest size class is simply

rounded up and designated as having equivalent diameters for objects within the range of 0.02 to 0.1 mm.

Perez et al. (2006) morphologically analysed the segmented floc objects of their study using the morphological parameters of equivalent diameter, 2-D porosity, convexity, compactness, roundness and fractal dimension. Correlation analysis of the morphological parameter values of the floc objects detected in the Pearson's product momentum correlation coefficient ( $rp$ ) was done to estimate linear correlations. Significant correlation between certain morphological parameter pairs has been found by the authors. For significant/high enough coefficient values, roundness as defined by the authors has been found to correlate with convexity and compactness (and vice versa), fractal dimension and convexity have also been observed to correlate well with each other.

The work by the same group of authors also investigated the effect of sample dilution on the size distribution of the objects detected and analysed. It has been found and verified by the researchers that with an increase in the dilution of the acquired activated sludge samples, the mean size of the flocs have been found to decrease in significant amounts. By their results the researchers concluded that the sludge sample for digital images acquisition should be prepared without previous dilution in order to obtain accurate measurements of the microbial flocs size (Perez et al., 2006).

The difference of morphology between flocs and filaments can be seen in their elongation degree and smoothness of boundary (Jenne et al., 2002). According to R. Jenne *et al.*, among parameters of aspect ratio, roundness, form factor, fractal dimension and reduced radius of gyration, the most accurate parameter in differentiating the two is the reduced radius of gyration (Jenne et al., 2002). The most unsuitable being the form factor followed by the fractal dimension. The result is obtained via a classification error comparison of 100 flocs and 100 filaments (manually identified).

Table 2.1 summarizes the literature review for image acquisition and image segmentation.

**Table 2.1: Literature Review**

No.	Literature Title	Type of Microscopy and Magnification	Sample Size on Slide and Number of Acquired Image	Segmentation Method
1.	Evaluation of activated sludge systems by image analysis procedures (Mesquita et al., 2008)	Brightfield, 100x	25uL , 200 total images	References no. 9
2.	Correlation between sludge settleability and image analysis information using Partial Least Squares (Mesquita et al., 2009)	Brightfield, 100x	25uL , 200 total images not including previous data	References no. 9
3.	Monitoring of activated sludge settling ability	Brightfield, 100x and 40x using	25uL , 200 images per	References no. 9

	through image analysis: validation on full-scale wastewater treatment plants (Mesquita et al., 2009)	stereo microscope	sample: & 20 images per sample for stereo	
4.	A comparison between bright field and phase-contrast image analysis techniques in activated sludge morphological characterization (Mesquita et al., 2010)	Brightfield and Phase Contrast, both 100x	25uL , 200 images total ~divided through three replicate slides; around 20 images obtained for each slide	References no.8 and no. 9
5.	Identifying different types of bulking in an activated sludge system through quantitative image analysis (Mesquita et al., 2011)	Brightfield 100x total; Epifluorescence microscopy 200x total	10uL for brightfield, 150 total images, 3 slides per sample, (3 x 50 images/slide) & 10uL for epifluorescence, 100 total images, 2 slides per sample, (2 x 50 images/slide).	References no. 8 for brightfield
6.	Characterization of activated sludge abnormalities by image analysis and chemometric techniques (Mesquita et al., 2011)	Brightfield 100x; Fluorescence microscopy 200x	Same as above	References no. 9 for brightfield work
7.	Quantitative image analysis for sludge volume index and total suspended solids prediction in activated	Brightfield and Phase Contrast 100x; Epifluorescence microscopy 200x	-	Not described

	sludge system disturbances (Mesquita et al., 2011)			
8.	Image Analysis in Biotechnological Processes: Applications to Wastewater Treatment (Amaral, 2003)	Brightfield 40x total for aggregates using stereo microscope and Phase contrast 100x for filaments	50uL for filament and aggregate, 18 images each 1-cover-slip-slide; 25 images for aggregate for sample, 30 images for filaments for sample	Use of boundary image segmentation and percentile based region image segmentation and then conjugating the resultant images to obtain aggregate/floc image, uses aggregate image to obtain filament image
9.	Activated sludge monitoring of a wastewater treatment plant using image analysis and partial least squares regression (Amaral et al., 2005)	Brightfield 40x total for aggregates using stereo microscope; Phase contrast 100x for filaments	50uL , 30 images per sample for filaments; 25 images per sample for aggregates	Similar algorithm as observed compared to no. 8
10.	Bulking sludge treatment by microscopic observation and mechanical treatment (Heine et al., 2000)	Not mentioned	-	Not described
11.	Early warning-system for operation-failures in biological stages of WWTPs by on-line	Not mentioned	-	Not well described

	image analysis (Heine et al., 2001)			
12.	Feature analysis of activated sludge based on microscopic images (Sikora et al., 2001)	Not mentioned	-	Variance Operator, Laplacian Operator, ...
13.	Investigation on filamentous micro-organisms in sludge foaming from pulp & paper mill wastewater treatment plant (Larptansuphaphol et al., 2010)	Phase contrast, 100x for low power work (filamentous counts, observing floc structures), 1000x for identification of filamentous organisms	-	-
14.	Simultaneously monitoring the particle size distribution, morphology and suspended solids concentration in wastewater applying digital image analysis(DIA) (Yu et al., 2009)	Microscope not used	40 images each sample	Software work as programmed by the NI Vision Assistant
15.	Characterisation of activated sludge by automated image analysis (Da Motta et al., 2001b)	Brightfield 100x	A series of at least 70 images	Complex algorithm that considers the variance of the grey-level histogram with steps briefly described



16.	Characterisation of activated sludge by automated image analysis : Validation on full-scale plants (Da Motta et al., 2002)	Series of 70 images (meso-scale visualisation at x100 magnification in brightfield), & of 50 images (macro-scale visualisation at x25 magnification, blackfield) for some samples		Similar to above and software work using procedures embedded within Visilog
17.	Impacts of morphological, physical and chemical properties on dewaterability of activated sludge (Jin et al, 2004)	Brightfield; floc size distributions determined by a Malvern Mastersizer/E instrument with a 300mm lens which measures particles in the range 0.9–546 um, uses light scattering.	-	-
18.	Impacts of structural characteristics on activated sludge floc stability (Wilén et al., 2003)	Same as 17 but not involving filaments	At least 10 images (100x magnification) were taken for floc fractal dimension analysis	Software work for calculating floc fractal dimensions via IMAGEJ

19.	Microbial community structure in activated sludge floc analysed by fluorescence in situ hybridization and its relation to floc stability (Wilén et al., 2008)	Phase contrast 10-40x lenses for floc; Phase contrast and Brightfield 60x inverted lens for microbial community structures of the flocs	>100 images for floc	Manual software work
20.	Use of image analysis in the study of competition between filamentous and non-filamentous bacteria (Contreras et al., 2004)	Phase contrast 1000x	10uL , 3 slides per sample, 3-5 image per slide randomly acquired	Software work using Global Lab Image 2.10 software
21.	Towards on-line quantification of flocs and filaments by image analysis (Jenné et al., 2002)	Phase contrast 1000x objective	-	Not described in detail, the used “novel automatic histogram-based thresholding method” combines the commonly used Intermeans algorithm with the calculation of extremes in the first and second derivative of the grayscale image histogram
22.	Activated sludge image analysis data classification: an LS-SVM approach (Gins et	Brighrfield 10x10	-	References work of Jenné et al. (2003)

	al., 2005)			
23.	Activated sludge morphology characterization through an image analysis procedure (Perez et al., 2006)	Brightfield 120x total	1 drop, 50 images per sample	Algorithm with segmentation step based in Zack algorithm for binarisation
24.	Image analysis to estimate the settleability and concentration of activated sludge ( Grijspeerdt et al., 1997)	Dark field microscopy 50x using stereo microscope; 25x for sludge floc size measurement	-	Software work using specifically developed software in Microsoft Visual C + +

It can be seen from the table that methods vary a lot according to teams of researchers. In many of the documentations the segmentation algorithms are not considered the main focus of study and hence have been only briefly explained and documented.

## CHAPTER 3

### MATERIALS AND METHODS

#### 3.1 Methodology Overview

In this chapter we shall discuss the experimental procedures. The parts for the procedures include:

- 1) Laboratory based work for data acquisition and physico-chemical tests and measurements
- 2) Software based work or the development of algorithms which encompass digital imaging segmentation and morphological parameter analysis of the floc and filament objects
- 3) Establishment of result correlation for the implemented physico-chemical methods and digital imaging methods

The flowchart describing the methodology for the research work is shown in Figure 3.1.

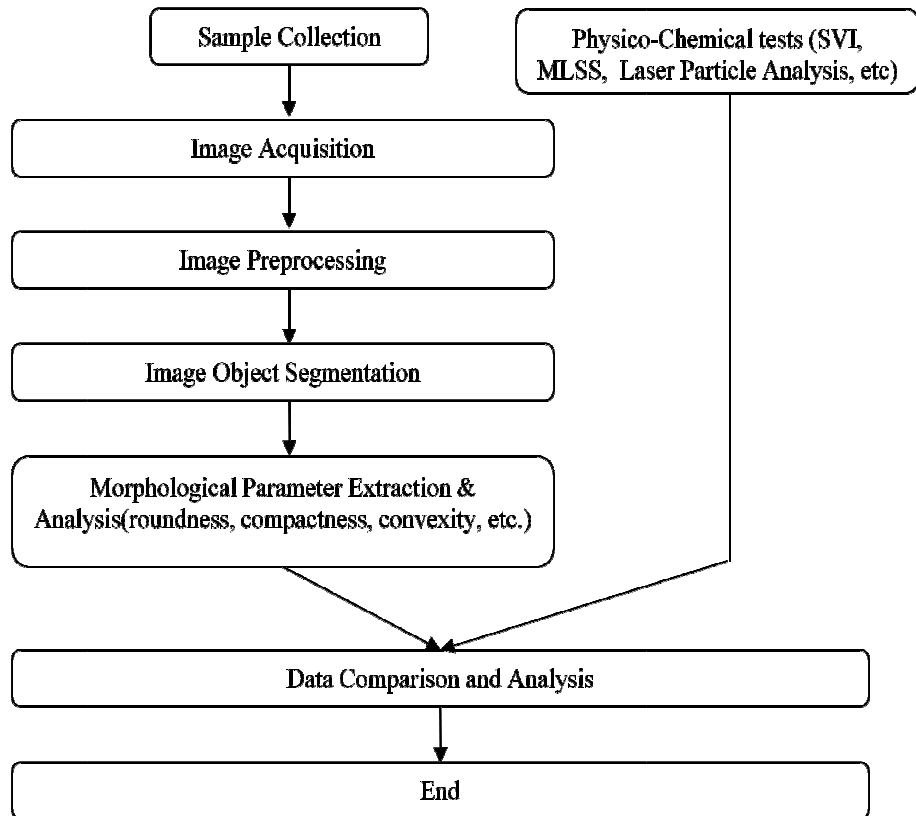


**Figure 3.1: Flowchart of methodology**

### 3.2 Image Acquisition

The samples of waste water are acquired from the activated sludge tanks of local wastewater treatment plants that deals with municipal effluents. For image acquisition a Zeiss Primostar microscope equipped with a CCD camera (Zeiss AxioCam ERC 5s) connected to a personal computer is used to capture the digital images. A sample is prepared simply by placing 80 $\mu$ l of activated sludge sample onto a microscopic slide using micro pipette and is then covered from the top with a 23  $\times$  23 mm cover slip. The sample is observed and up to 100 and more images are captured under the objective magnification of x4 for mainly floc

observations and analysis and x10 for filament observations and analysis filaments both in brightfield microscopy. The simulation platform is a laptop computer with Intel Centrino Duo Intel 1.66GHz CPU. MATLAB software is used for programming. All images are saved in JPEG file format. The image resolution is 1920 x 2560 pixels.

For the ‘floc’ algorithm, a total number of 55 images for each day/sample, half the number of the total number of roughly 110 images captured covering the entire cover slip area are used as inputs and processed. For the ‘filament’ algorithm, from the entire set of roughly equivalent number of captured images when snapped in a way that covers the whole cover slip area for a day/sample, the number of inputs for a day averages to about 52.

A sample ‘floc’ image in x4 from a sample is shown in Figure 3.2.

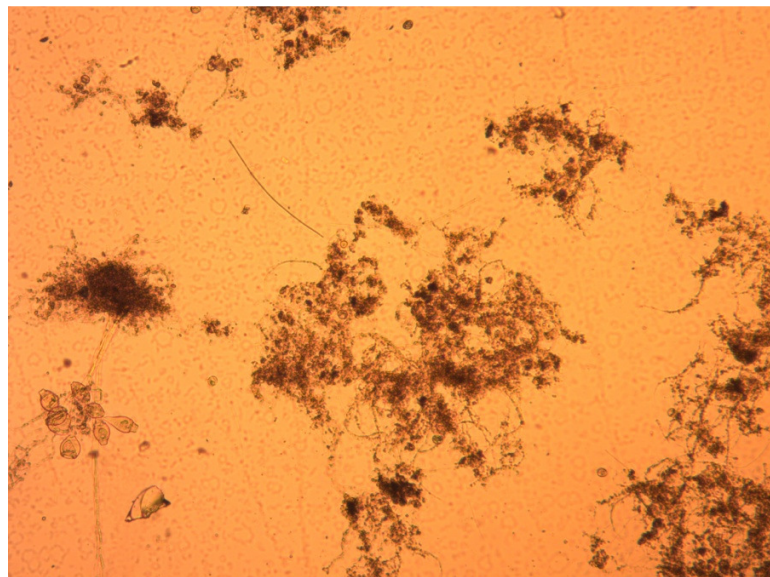


**Figure 3.2: Sample ‘floc’ image with x4 objective magnification**

Another image in x10 is shown in Figure 3.3.

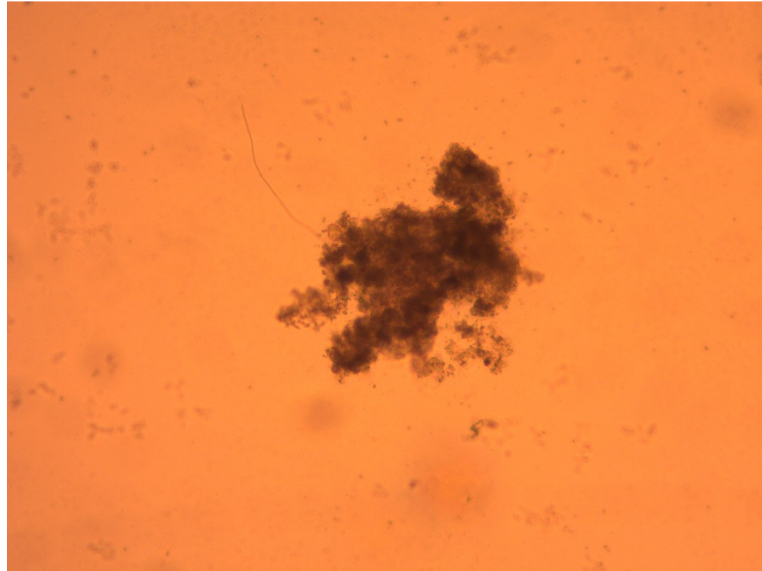


**Figure 3.3: Sample ‘filament’ image with x10 objective magnification**

In Figure 3.2, a pixel is equivalent to 0.838 micrometer in its length in both horizontal and vertical axis while in Figure 3.3, it is equivalent to 0.332 micrometer.

### **3.3 Physico-Chemical Tests**

The Malvern Mastersizer MS2000 laser particle size analyzer is used in this work for laser particle size analysis. A refractive index of 1.04 has been chosen for the samples as according to the consideration that the refractive index of the samples is to be very close to that of water ( $n < 1.05$ ) (Waite *et al.*, 1998). The physico-chemical tests of SVI, and MLSS or TLS are also carried out simultaneously on the same day which activated sludge samples are collected.

### **3.4 Floc Segmentation Algorithm**

#### **3.4.1 Stepwise Flow**

##### **1. Input Original Color Images**

The images acquired from samples wastewater treatment plants are used as inputs. The images otherwise known as ‘floc images’ have been captured in x4 objective magnification for containing the flocs.

##### **2. Grayscale transform of Images**

The images are transformed into grayscale forms with the threshold value obtained via the Otsu thresholding method.

##### **3. H-minima transform**

A value of 50 is used for the scalar threshold variable that determines the depth of difference.

##### **4. Implement Median Filtering**

A size of 25x25 for the window /filter is used.

##### **5. Implement Average Filtering**

A size of 50x50 for the window/filter is used.

##### **6. Local Thresholding Binarisation**

The ‘Niblack’ Method is chosen and used here with window size of 500x500,  $k$  value of -0.2 and offset value of 5.



### 7. Clearing of Border-attached objects

Incompletely captured objects are deleted after this the implementation of this step.

### 8. Removal of Small Objects

Image segmentation noise is cleaned off by removing objects smaller than a total area of around 2500 pixels. The exact number of pixels used as the variable number is 2457 as is equivalent to 0.05% of the total number of pixels found within an input image.

The overall flowchart of the floc algorithm can be seen in Figure 3.4.

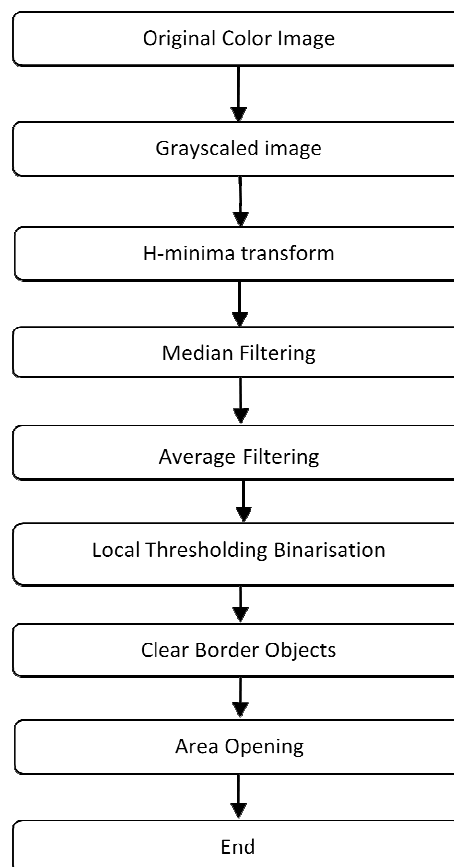


**Figure 3.4 Flowchart of floc segmentation algorithm**

### **3.4.2 Explanations and Elaborations**

In the proposed algorithm the H-minima transform is used. This operation eliminates the regional minima in the images that have an intensity/depth less than a given thresholding value. A smoothing effect is to be observed from the result of this operation. As the first step of the algorithm, the filament objects are still present and visible after the operation is complete.

It is observed that at x4 objective magnification, the filaments are very thin and threadlike. Median filtering with a moderately large window size is then applied to the resultant image to effectively and efficiently eliminate the thin filament objects. Median filtering is followed by an average filtering process to further smoothen the image.

Next, a local thresholding binary conversion in the Niblack method produces the segmentation result 'floc' image.

Local thresholding/adaptive thresholding, as opposed to global thresholding methods that treats the entire image as a whole, computes the threshold value for each pixel by using the values of all pixels contained within the same local window. As such, the process repeats for different localities until the window covers the entire image. Niblack local thresholding (Niblack, 1986) is

a simple and elegant technique that was originally developed for document/text images. The threshold value is obtained by first calculating the local mean and then a value is added to the result depending on the local standard deviation. Assume that by narrowing the processing scope by processing local areas instead of the entire image, the pixel intensity value variation of both objects and background hence gets narrowed so and such that the graph model of two peaks/clusters becomes valid for the pixel intensity value histogram, and also that local background pixels are always significantly larger in number than foreground/object pixels, the mean can be seen to fall within the range of the background intensity values; and to move the mean outside of the background intensity value range, the standard deviation value is utilized.

$$T_{\text{Nblack}} = \text{mean} + k \times \text{standard deviation} - c \quad (3.1)$$

The value of  $k$  is positive for bright objects and negative for dark objects since the direction of movement is determined by the variable. Normally the value of  $0.2/-0.2$  is chosen as the optimum value. 'C' represents an offset variable. As have been stated in the previous section, the values of 'k' and 'c' are set to  $-0.2$  and  $5$ , and the window size used is  $500 \times 500$ .

### **3.5 Filament Segmentation Algorithm**

#### **3.5.1 Stepwise Flow**

##### **1. Input Original Color Images**

The images snapped and saved in the previous sessions are used as inputs. The images otherwise known as 'filaments images' have been captured in x10 objective magnification for containing the filaments.

##### **2. Grayscale transform of Images**

The images are transformed into grayscale forms with the threshold value obtained via the Otsu method.

##### **3. H-minima transform**

A value of 30 is used for the scalar threshold variable that determines the depth of difference.

##### **4. Implement Median Filtering**

A size of 25x25 for the window/filter is used.

##### **5. Morphological Erosion**

Disk structural element with a 10-pixel-radius is used.

##### **6. Addition of Images from Step 3 & Step 5**

The Eroded image from step 5 is complimented and added with the image from step 3. Images containing only the filament regions are produced after this step.

#### 7. Binary Conversion

The image from the previous step is binary converted using the Otsu method.

#### 8. Implement Average Filtering

A size of 50x50 for the window/filter is used.

#### 9. Local Thresholding Binarisation

The 'Niblack' Method is chosen and used here with window size of 500x500, k value of -0.2 and offset value of 5.

#### 10. Morphological Dilation

Disk structural element with a 10-pixel-radius is used.

#### 11. Imposition of Enlarged Floc Object Areas

The steps starting from no. 8 form the continuation of the developed floc algorithm leading to the current step to further reduce the noise of the input image to be used for the next following step 12.

#### 12. Implement Hough Transform for Straight Line Detection

This step makes dots and lines that seem like broken parts of a larger straight line to connect together to restore the line.

#### 13. Morphological Parameter Filtering of Images from Step 7 & Step 12

The morphological parameter of 'Roundness' is used here with a threshold value of 0.15.

#### 14. Merging of Both Images from Step 13

The images are merged with each other producing segmentation results that incorporate existent regions from both inputs. The logical OR operation is used in this step.

The overall flowchart of the filament algorithm can be seen as in Figure 3.5.

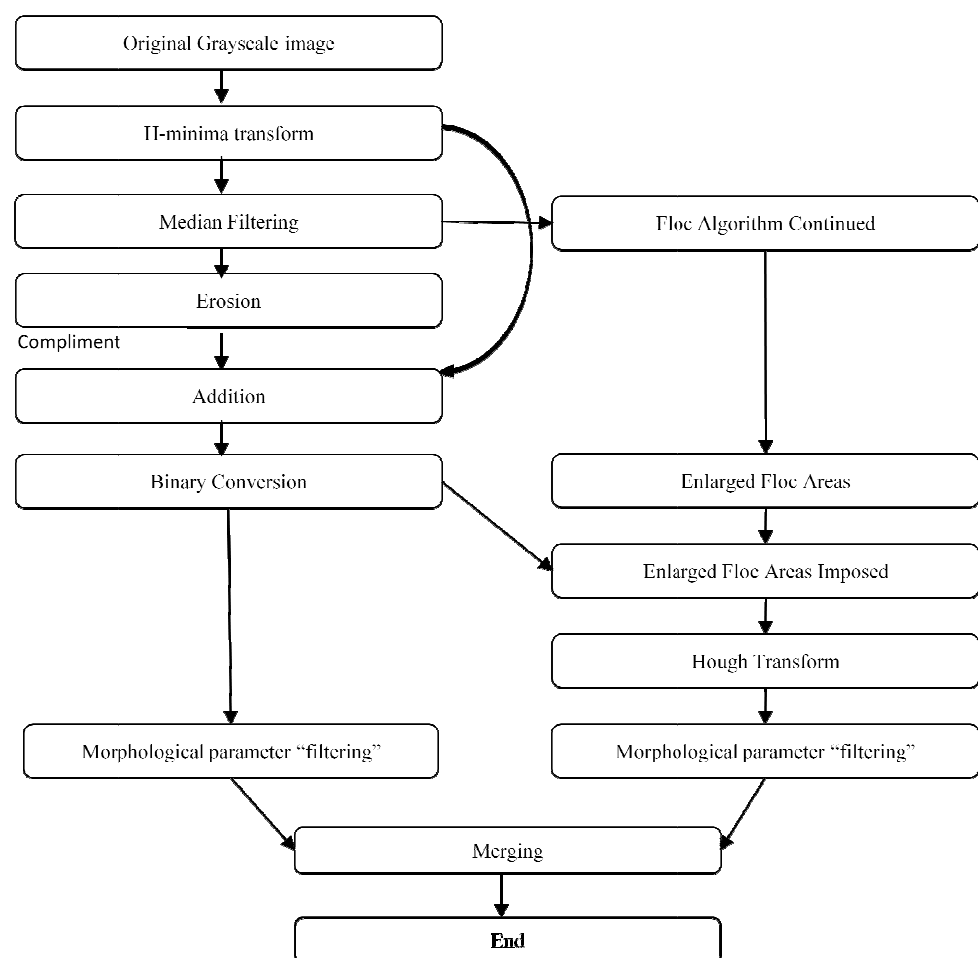


**Figure 3.5: Flowchart of filament segmentation algorithm**

### 3.5.2 Explanations and Elaborations

The 'filament' algorithm developed here incorporates the 'floc' algorithm that has already been developed.

The H-minima transform operation of step 3 produces here again a smoothed image but with the filament objects still intact. A threshold value of 30 has been used instead of 50 as in floc segmentation algorithm for even more preservation of filament objects.

The next median filtering operation erases the filament objects from the images.

The erosion operation of step 5 is a grayscale erosion operation. Grayscale erosion operations selects for an image pixel the lowest value of intensity found for all the pixels covered by the selected structuring element with its centre pinned on the aforementioned pixel. The overall after effect is of a darkened image with dark regions enlarged and light regions eroded.

For step 6, the complement of the resultant image from step 5 and the image from step 3 are added together to produce the output image. The former image can be termed the 'floc' image while the latter be termed the 'floc & filament' image. There are three types of regions involved in the process. The first region is the one representing the floc object areas, the second region the one

representing the filament areas and the third region is the background region having neither floc nor filament. The 'floc' image whether complemented or not has no region 2 but only the first and the third regions. Region 1 and 3 are roughly identical with each other in both the 'floc' image and the 'floc & filament' image. The complemented 'floc' image when added to the 'floc & filament' image overloads pixel intensity values of region 1 and 3 to become over/more than 255. The pixels from region 2 however get added with intensity values that do not push them over 255. The end result is that only filament object regions are retained/left behind after step 6.

For as large as possible a matching between the areas and pixel intensity values of region 1 and 3 from the 'floc' image and the 'floc & filament' image, no significant altering or changes are to be done after the median filtering step which eliminated the filaments. In such a way the highest possible fidelity and matching is to be obtained and achieved. The Erosion step serves as a semi-insurance-step to make the intensity values that get added in the addition step becomes slightly larger than the values otherwise, making for perfectly reaching the 255 threshold so that overloading is definitely reached for the necessary areas. A moderately large structuring has been chosen so that significant darkening can occur but not too large that the floc object regions get too enlarged.



After the subsequent binary conversion, the operation at the left-hand-side of the flowchart of Figure 3.4 comes to an end. This concludes the first segment/section of the algorithm.

From the first part of the algorithm, we can see that the algorithm is robust across different background lighting conditions and textures due to step no. 6 described. For this important consequence to happen the usage of the median filter also plays an indispensable role because as long as the filaments captured are thin and threadlike, they would be eliminated after the operation regardless of the intensity difference between their pixels and the background pixels. Overall there needs to be no care taken to ensure a constant background lighting condition when performing image acquisition/capturing at all by operators.

For the second part of the algorithm, the right-hand-side of the flowchart starts with continuing with certain parts of the developed floc segmentation algorithm. Average filtering continued by the Niblack local thresholding is implemented. After then to bulk up the floc objects thus detected, a morphological dilation process is performed.

The enlarged floc objects are then imposed on the image produced by step 7 for noise reduction.

Next, the Hough transform operation for detecting straight lines is applied to the resultant image. Through the Hough transform, unconnected single dots and dots at the edge of a shorter line that form larger straight lines become connected with themselves and with each other (restoring the line) if the accumulated quantity of dots for a possible line/longer line is found to be greater than the set threshold value.

Any straight line can be defined by the form:  $y = mx + c$  in the Cartesian coordinate system where  $m$  and  $c$  are constants that define the lines while  $x$  and  $y$  are the point coordinate variables. By tallying the quantity of the  $x$  and  $y$  value pair that fits into any particular  $m$  and  $c$  value pair, it can be seen that sufficient such quantity indicates either an already existing straight line or one such line to be connected. Connected parts of a line will have continuous  $x$  and  $y$  value pairs while unconnected ones will not; the unconnected sections to be joined together by this operation provided that the separating distances/gaps are not too large.

The basic concept for Hough transform for line detection described above can be explained in another way that describes conversion from the  $(x, y)$  space to the  $(m, c)$  space. In this case the  $x$  and  $y$  value pairs described above are represented as dots of lines crossing each other in the  $(m, c)$  space, while continuous value pairs indicate continuous gradient of different lines.

The actual implementation of the Hough transform for line detection as is done in Matlab uses yet another form of representation, creating the ‘Hough space graph’ with waveform curves representing each dot/ data point of the  $(x, y)$  space. Again different curves crossing at any one spot indicates a possible line. Such crossings at any one spot are to be accumulated and then thresholded for the determination of line existence.

Also, the Cartesian coordinate system comes with the inherent problem of having vertical lines defined by an infinite value for the slope/ gradient variable of  $m$ . Therefore the Hough transform is by default implemented using the Polar coordinate system.

By making the resultant connected lines into binary images, the resultant binary image of the Hough transform as well as the image from step 7 both go through the morphological parameter filtering operation next.

The parameter employed here is roundness. It is used here to eliminate the segmented binary regions that are not sufficiently elongated. Roundness is defined here as the ratio of an object’s area to a circle/disc’s area with the circle/disc equal in length to the object. It is as follows:

$$\text{Roundness} = \frac{4 \times \text{area}}{\pi \times \text{length}^2} \quad (3.2)$$

The roundness of an object as defined above varies from a value of 1 for a circle to values closer to zero for increasingly elongated objects in a similar layout

fashion found in an image. For our purposes, ‘elongation’ used here indicates object length in a way that do not consider a line in a more compact layout as less elongated than another one layout of it in which it is straight; at the same time however, the differences in roundness values caused by the differences in layouts are not considered as significant enough. The ‘length’ term of equation (3.2) is defined as the major axis length, which is the length of the major axis of the ellipse that has the same normalized second central moments as the object. Only objects with roundness values lesser than the value chosen in both images indicating they themselves as long objects remain after the operation.

The usage of the Hough transform has enabled unconnected dots that potentially form filament lines to be connected with each other. Unconnected round dots are to be eliminated if processed by step no. 13 skipping step no. 12 but they remain and stay if the Hough transform operation caused them to be connected to an extrapolated line which is judged to be a filament in our case. At the same time however, we can expect new noise in the form of fake filaments or connected lines that are not filaments added into the result. To compensate for the drawback, the floc objects had been explicitly detected using the developed ‘floc’ algorithm as well as dilated to enlarge them and then imposed on the image of step 7 to eliminate the existing dots originating from the floc objects. This step however, also breaks up certain previously-connected filaments even when unenlarged floc objects are used for imposition. The final merging step allows for

the detected lines from both branches to meet and combine providing for a more comprehensive image/segmentation result.

The result gives the segmented filaments.

### 3.6 Assessment of Segmentation Accuracy

For verifying the segmentation accuracy of the algorithms, ground truth images have been hand-drawn using the software GIMP with the original color images as reference or base. The overlapping of the images from manual drawing (ground truth) and algorithm output produces true positive, false positive, true negative and false negative areas. Segmentation accuracy values via various metrics may be obtained therefor by calculation using their area values.

The Dice's coefficient metric (also known as the Sørensen index among other names) that is commonly and extensively used in image segmentation quality validation is utilized in our study and is defined as below:

$$\begin{aligned} DC &= \frac{2 \times TP}{2 \times TP + FP + TN} \\ &= \frac{2 \times TP}{TP + \text{All\_Areas}} \end{aligned} \quad (3.3)$$

where TP=True positive, FP=False positive and TN=True negative.

The study of Zou et al. (2004) finds the Dice coefficient “a simple and useful summary measure of spatial overlap, which can be applied to studies of reproducibility and accuracy in image segmentation”.

### 3.7 Morphological Parameters for Analysis of Floccs

Morphological parameter analysis involving the four parameters of equivalent diameter, roundness, compactness and convexity are done after the objects have been segmented. These morphological parameters have been chosen as they describe different properties of circular objects. Their definitions can be seen as follows:

Equivalent diameter= the diameter of a circle with an equivalent front facing area;

$$\text{Roundness} = \frac{4 \times \text{area}}{\pi \times \text{length}^2} \quad (3.4)$$

$$\text{Compactness} = \frac{4\pi \times \text{area}}{\text{perimeter}^2} \quad (3.5)$$

$$\text{Convexity} = \frac{\text{area}}{\text{convex hull area}} \quad (3.6)$$

More documentations and discussions of the analyses conducted after the successful object segmentation process can be found in the succeeding Chapter 4.

## **CHAPTER 4**

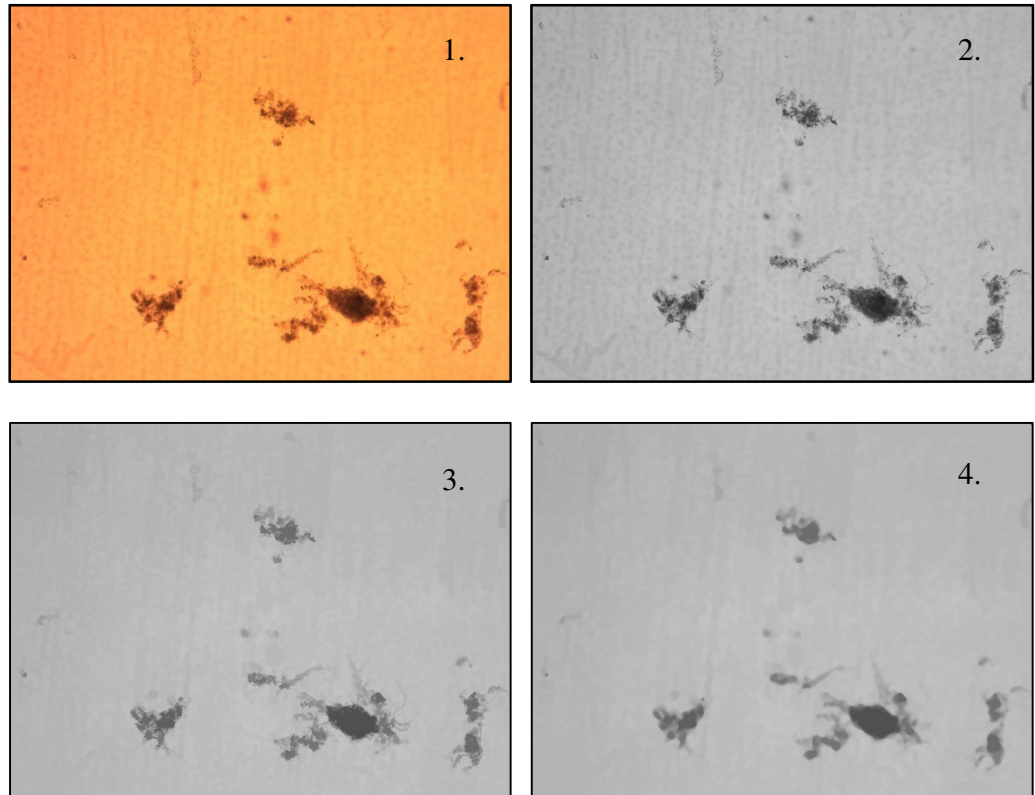
### **RESULTS AND DISCUSSIONS**

In this chapter we will discuss the results of the proposed algorithms as well as the algorithm segmentation accuracy. The subsequent analyses utilizing results from image processing and physico-chemical methods will then be gone through and discussed.

#### **4.1 Step by Step Output Images**

##### **4.1.1 Floc Segmentation Algorithm**

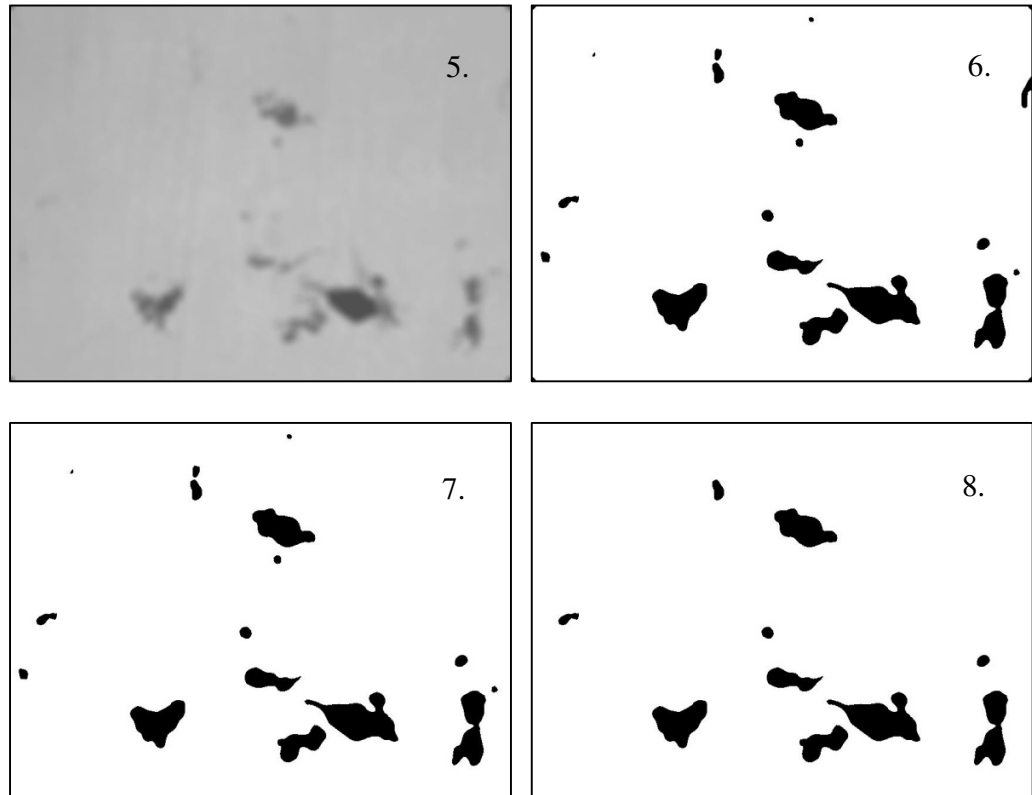
The output images for each of the step of the developed floc algorithm can be seen in Figure 4.1. For all 6 samples 55 images are processed by the algorithm out of the total number of approximately 110 images covering the entire area of the microscopic cover slip.



1: Original input color image; 2: Grayscale image;  
3: H-minima transformed image; 4: Median filtered image

**Figure 4.1 (Continues on next page)**





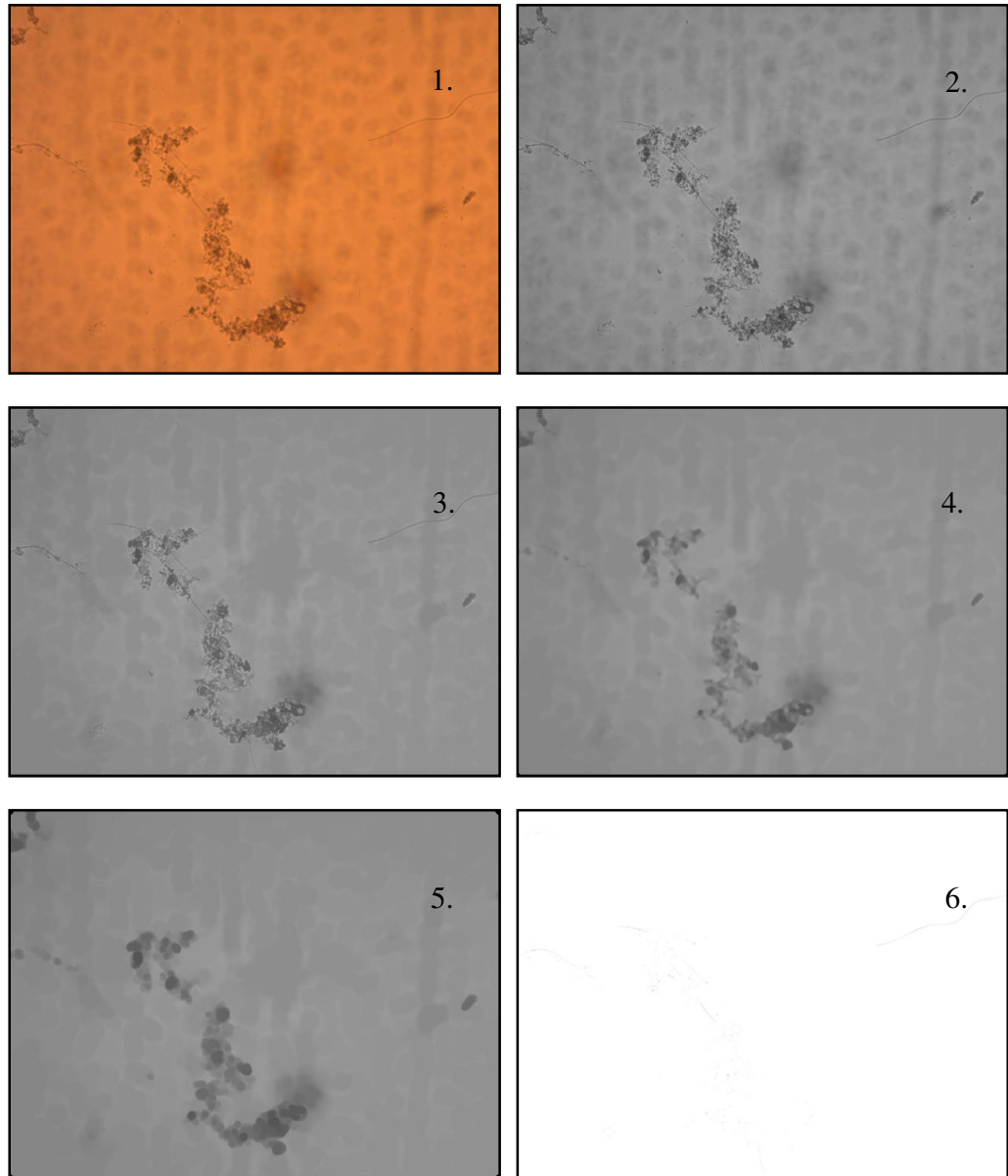
5: Average filtered image; 6: Local thresholding binarisation;  
7: Clearing of border objects; 8: Small object removal

**Figure 4.1: Steps of floc segmentation algorithm**

The output image of step 8 shown is the complement of the actual black-background-white-object image for better visualisation.

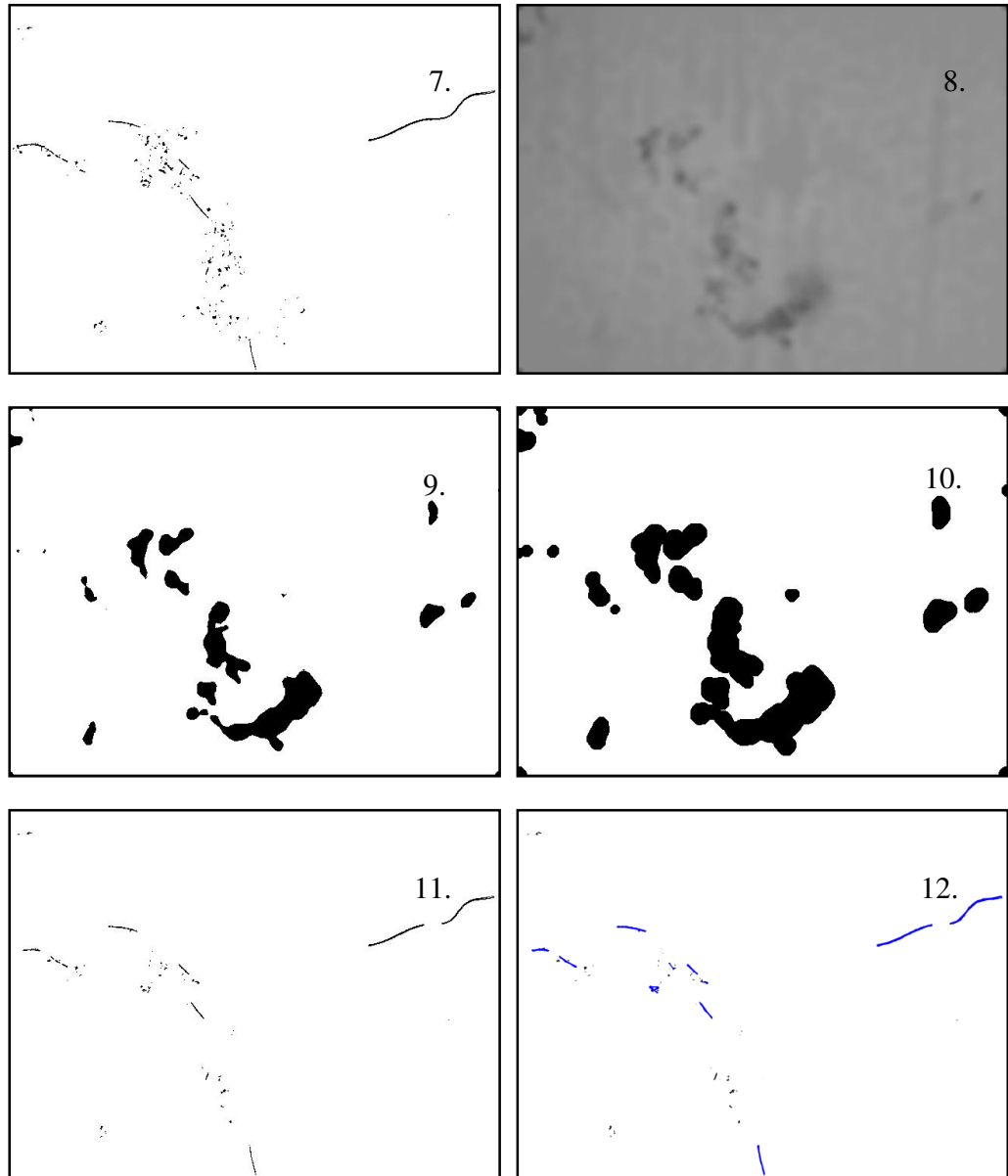
#### **4.1.2 Filament Segmentation Algorithm**

The output images for each of the step of the developed filament algorithm can be seen in Figure 4.2.



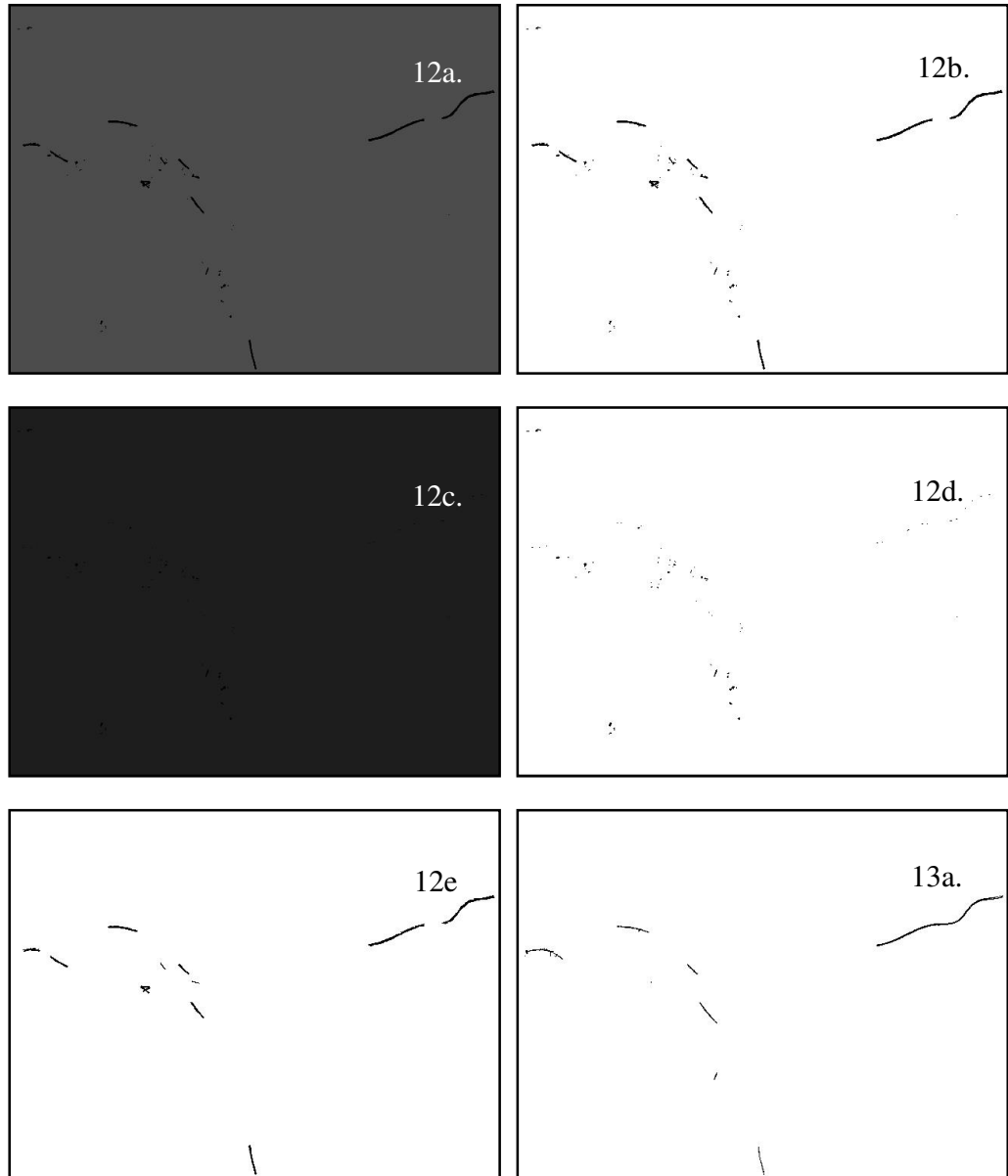
- 1: Original input color image; 2: Grayscale image;  
3: H-minima transform image; 4: Median filtered image;  
5: After grayscale morphological erosion;  
6: Addition of image 3 and image 5 complemented

**Figure 4.2 (continues on next page)**



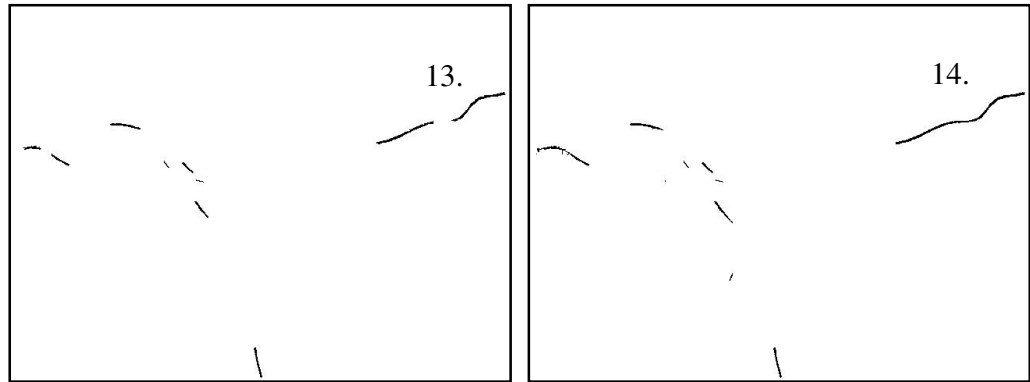
7: Binarized image, 8: Average filtering applied to image 4;  
 9: Local thresholding binarization; 10: Morphological dilation;  
 11: Image 10 imposed on image 7;  
 12: Implementation of Hough transform for line detection;

**Figure 4.2 (continued)**



12a: Grayscalezation of image 12 in RGB red channel; 12b: Binarized image;  
 12c: Grayscalezation of image 12 in RGB blue channel; 12d: Binarized image;  
 12e: Binary image of detected lines by Hough transform;  
 13a: Short objects eliminated from image 7;

**Figure 4.2 (continued)**



13b: Short objects eliminated from image 12;

14: Merging of image 13a and 13b;

**Figure 4.2: Steps of filament segmentation algorithm**

The output images of step 10, 13 and 14 are the complement of the actual black-background-white-object images for better visualisation. The image from step 12 has the lines connected by the Hough transform plotted in blue color. With the image from step 12 as input, 12a is the image with only the red RGB channel activated and then converted to grayscale and 12b the subsequent binarization result. 12c is the image with only the blue RGB channel activated and then converted to grayscale and 12d the following binary converted result.

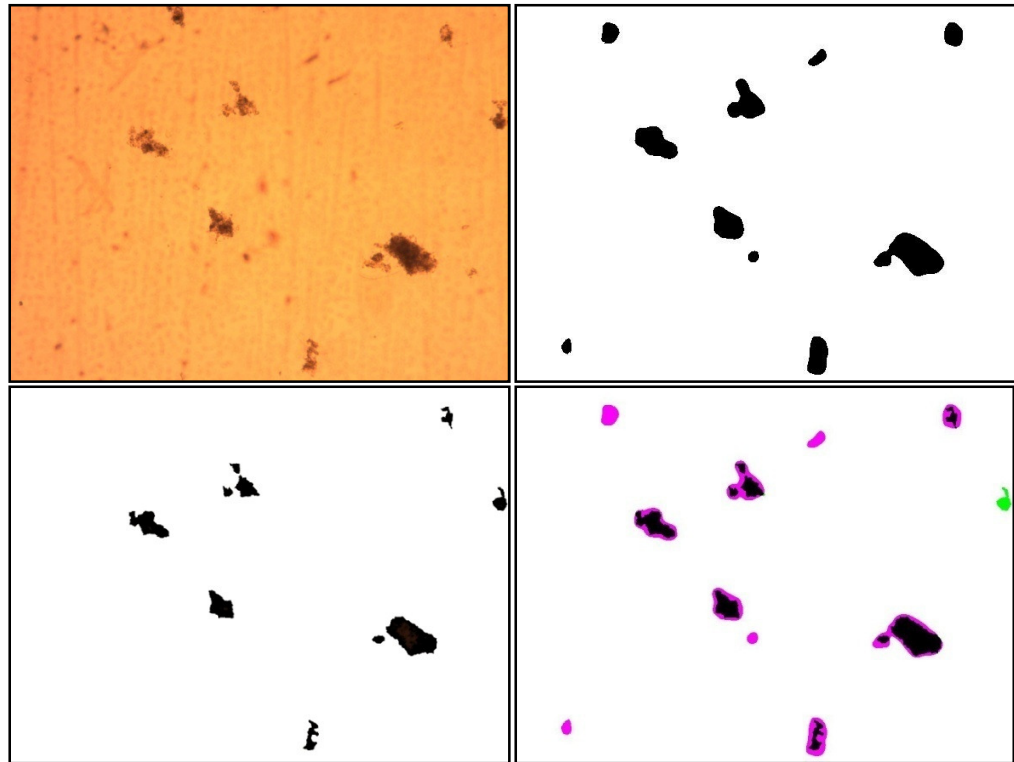
Activating only the red channel for the input image makes blue regions black and white regions red while black regions remain the same. Activating only the blue channel makes white regions blue while blue and black regions remain the same. Thus, merging the two binary outputs from the previous steps via logical operation give us an end image that is binary with its black regions

representing the blue regions of the Hough transform processed image. 12e shows this image. Further processing this image with morphological parameter filtering gives 13b and 13a has the image from step 7 as input.

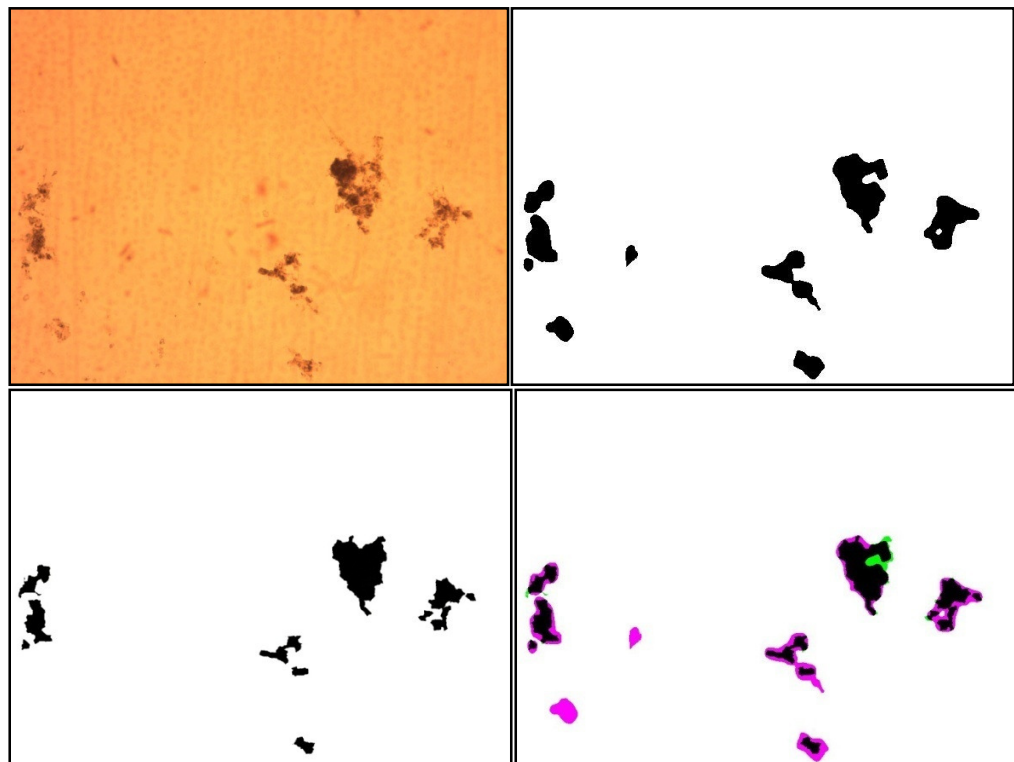
#### **4.2 Ground Truth Flocc Segmentation Accuracy Test**

For assessment, Figure 4.3 shows sets of images of 4 for each different input. The top left shows the original color image, the top right shows the segmented image, the bottom left shows the ground truth image and the bottom right image shows the combined image for assessment.

The Dice coefficient value is calculated and displayed under each of the set of images.

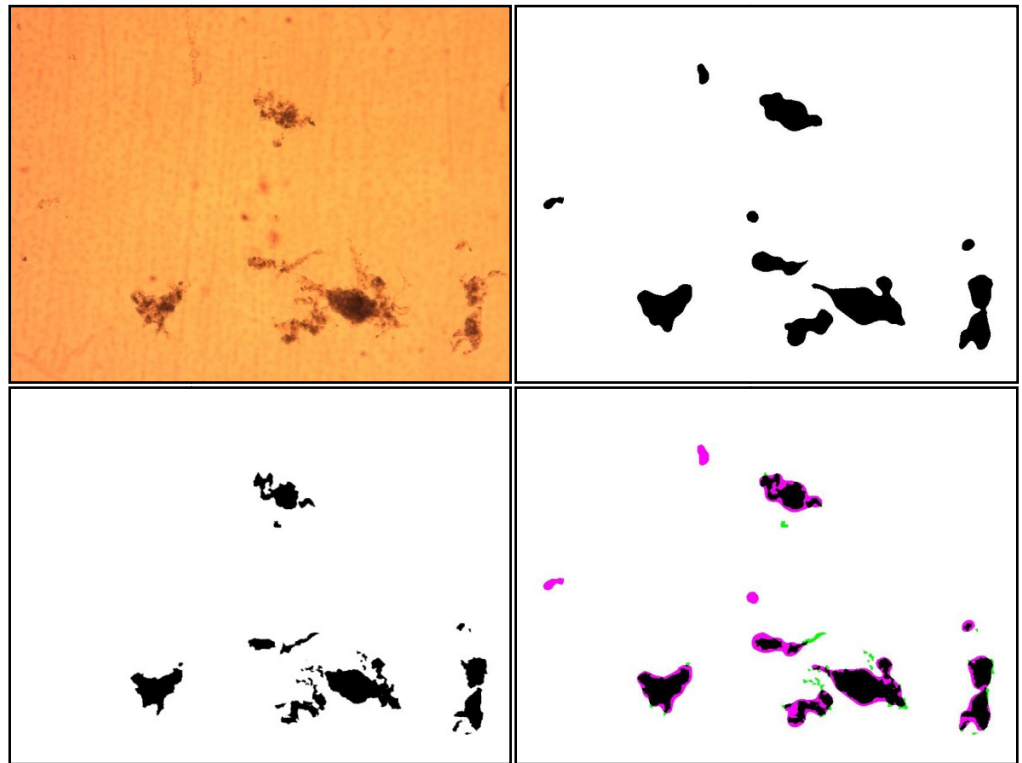


(a)  $DC=2*64364 / (64364+143484)= 128728 / 207848= 61.9337\%$

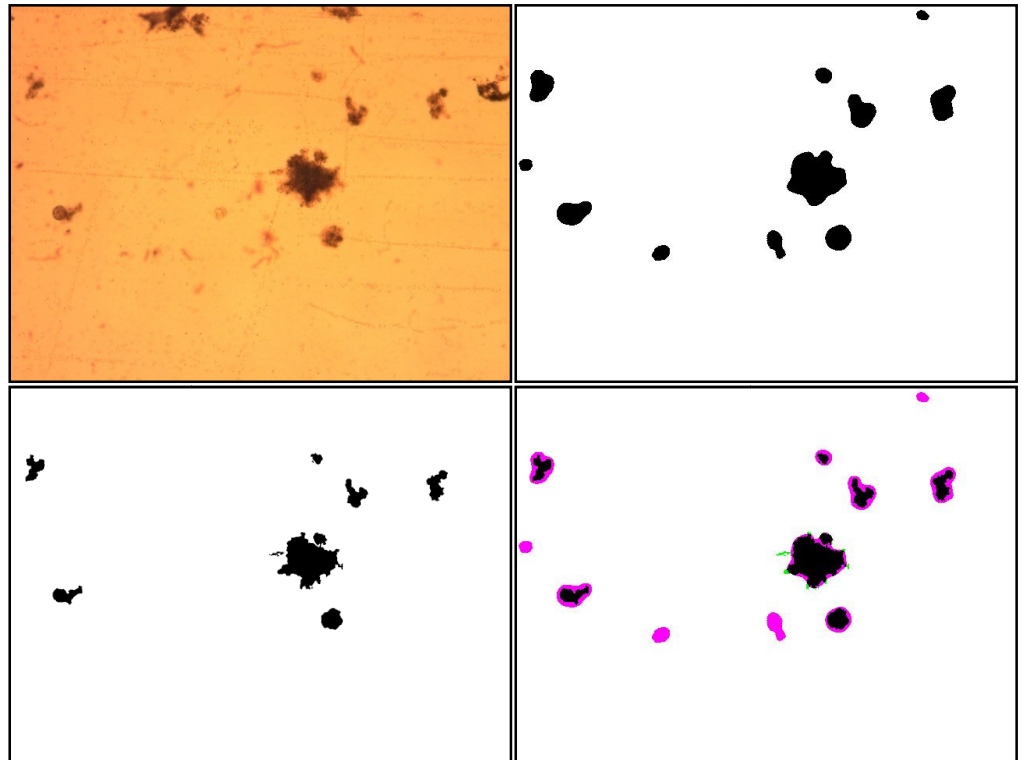


(b)  $DC=232838 / 319952 = 72.7728\%$

**Figure 4.3 (continues on next page)**



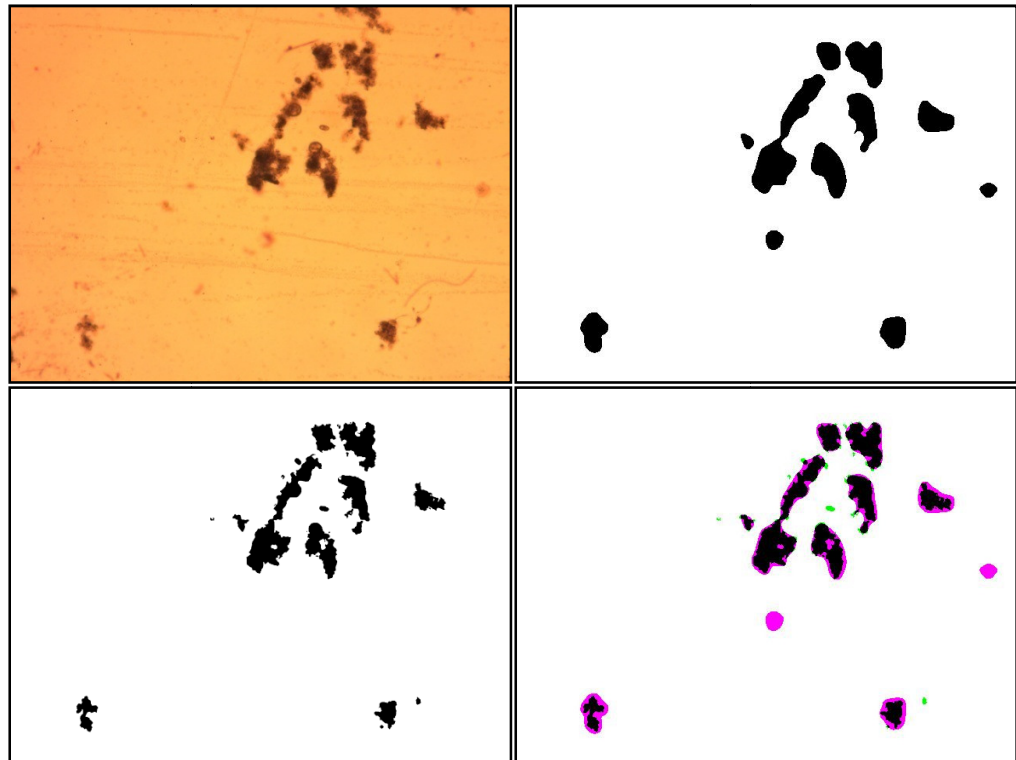
(c) DC = 74.1818%



(d) DC=70.8605%

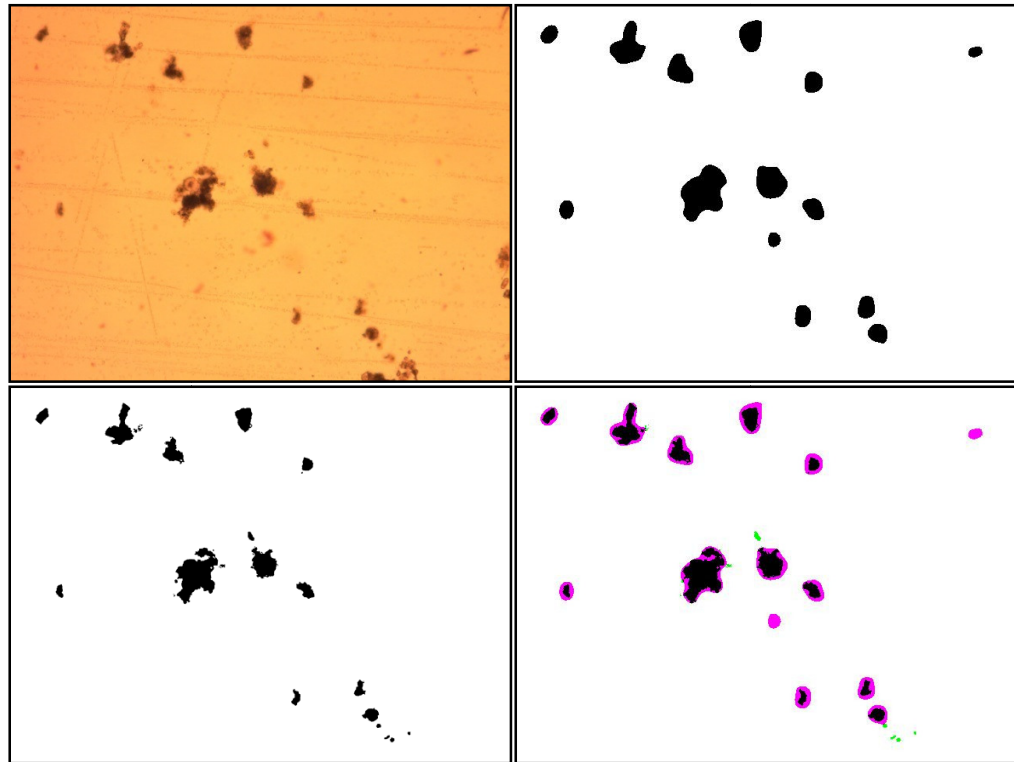
Figure 4.3 (continued)





(e) DC=81.1048%

Figure 4.3 (continues on next page)



(f) DC=70.2651%

**Figure 4.3: Assessment of floc segmentation**

Top Left: Original colored image, Top Right: Segmentation image,  
Bottom Left: Ground truth image, Bottom Right: Assessment image

The assessment images shown above have black regions representing overlapping regions between segmented objects and ground truth image, pink regions representing regions present in the segmented objects but not in the ground truth image, green regions showing the regions existing in the ground truth image but not in the segmented objects and finally the white regions representing non-object regions in both inputs.

In ground truth verification terminology the representations are as follows:

- **Black regions: Overlapping regions** - **True Positive**
- **Pink regions: Segmented regions only** - **False Positive**
- **Green regions: GT regions only** - **True Negative**
- **White regions: Background regions** - **False Negative**

From a visual qualitative judgement perspective, the segmentation algorithm can be seen to be quite successful. The images used for algorithm input are generally as seen as above, where they are quite noisy and in many cases it is difficult to differentiate between floc and noise.

For the first set of images used, the green object at the right hand side seen to be touching the border has been classified as such in ground truth image drawing via eye assesment. However, it seems that the object is not really touching the border from the algorithm processing especially if the upper part of the object is counted out. The accuracy of the segmentation for the first set is expected to increase significantly if that object is not taken as a border object in ground truth image making.

The accuracy values from Figure 4.3 are displayed in Table 4.1.

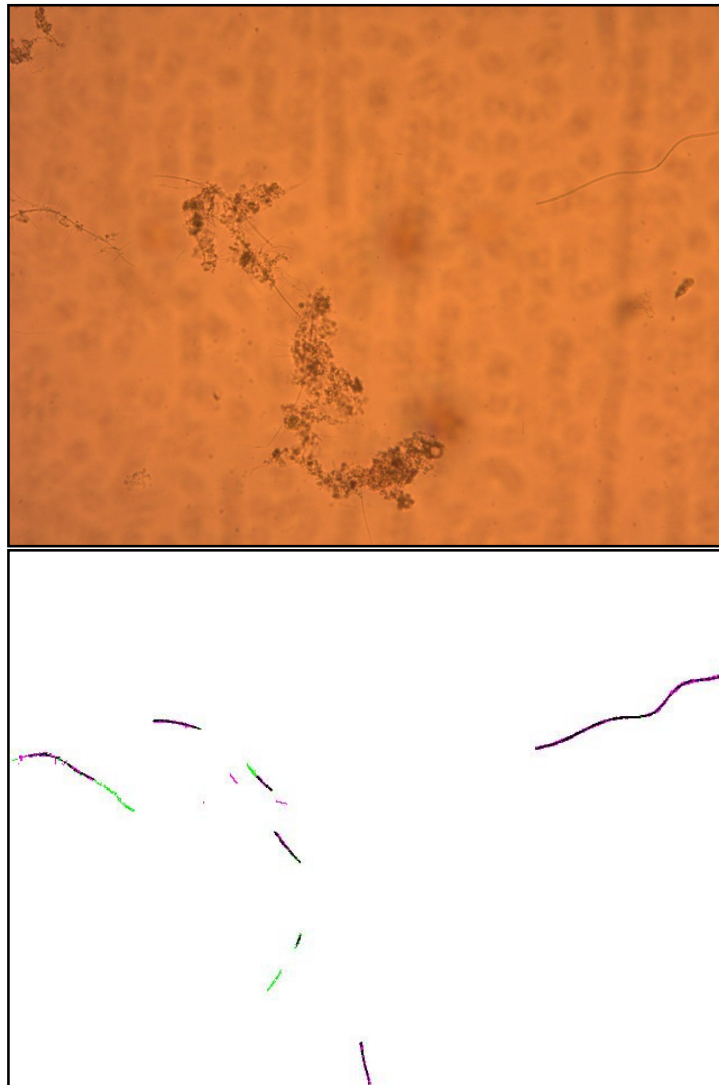
**Table 4.1: Dice Coefficient Values for Floc Images**

Image	Accuracy(Dice Coefficient)
a	61.9337%
b	72.7728%
c	74.1818%
d	70.8605%
e	81.1048%
f	70.2651%
Average	71.8531%

From the images in Figure 4.3, an average accuracy value of 71.85% is calculated. An accuracy of above 70% has been achieved, quantitatively the segmentation can therefore be judged to be good.

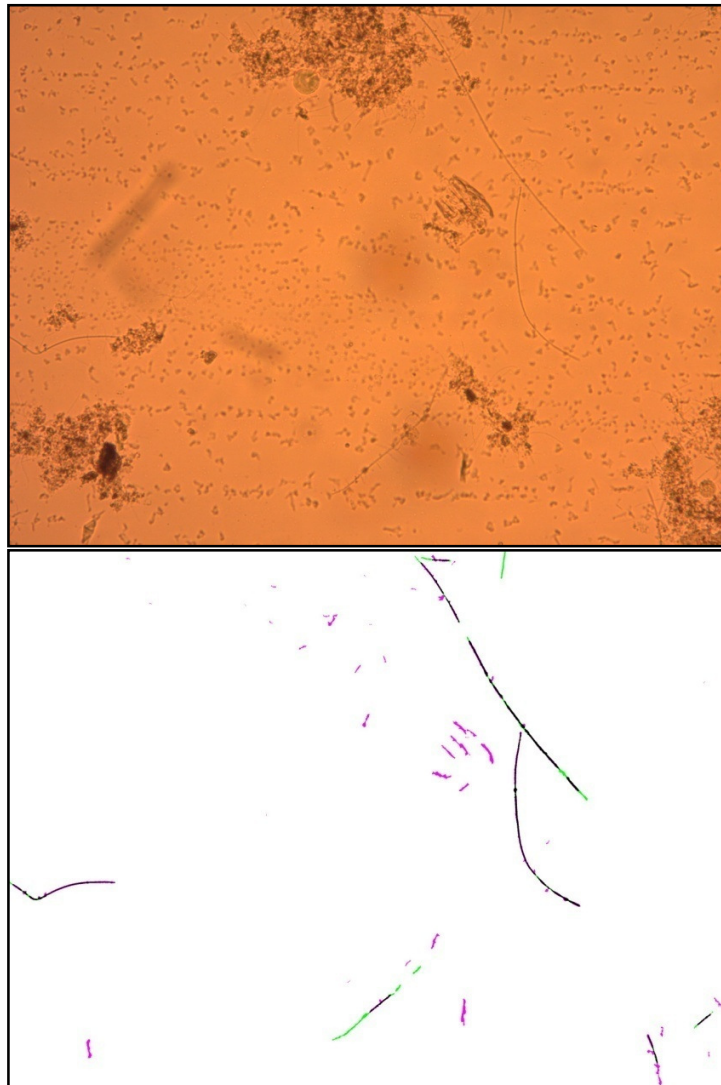
#### **4.3 Ground Truth Filament Segmentation Accuracy Test**

The assessment of the filament segmentation accuracy in the Dice's coefficient criterion can be seen in Figure 4.4.



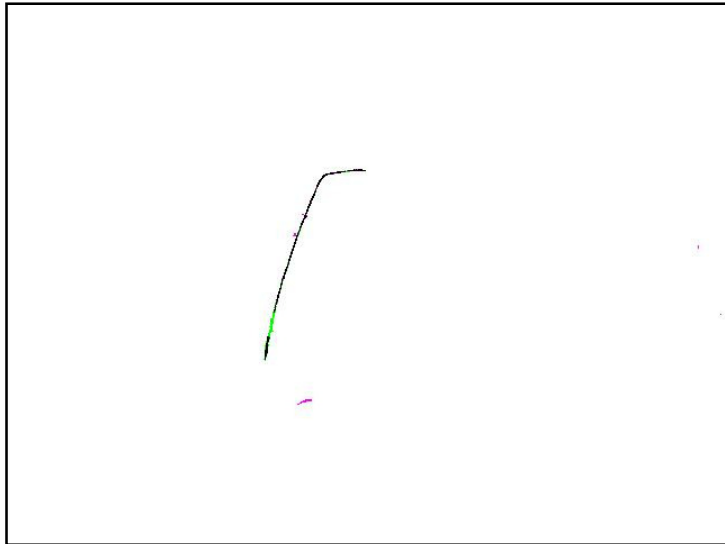
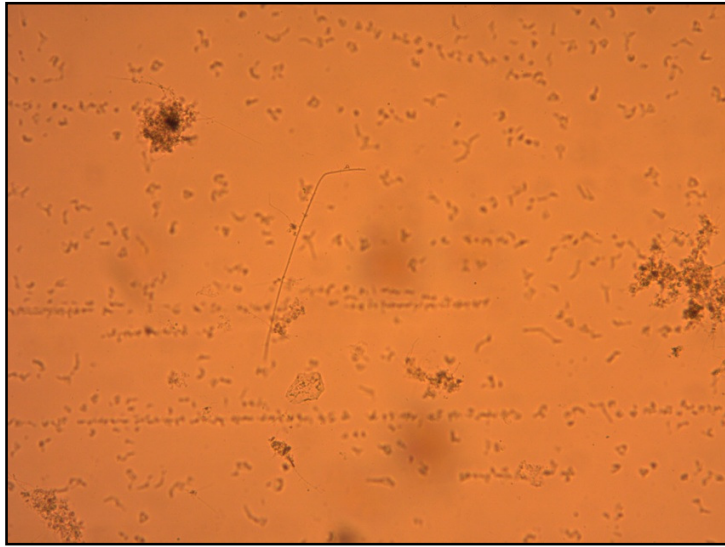
(a)  $DC=2*10017/(10017+20781)=20034/30798=65.0497\%$

**Figure 4.4 (continues on next page)**



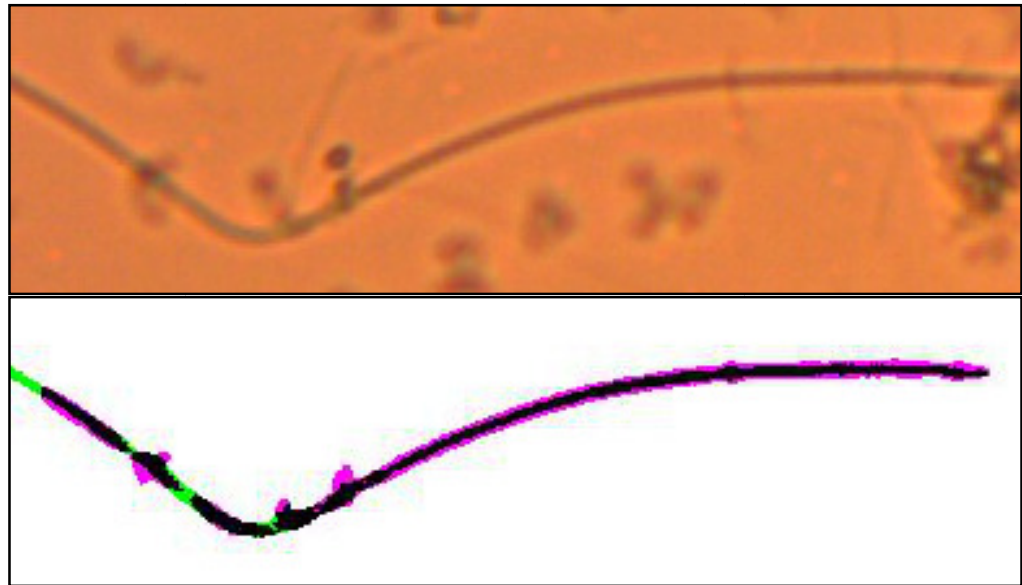
(b)  $DC=2*13380/(13380+30886)= 60.4527\%$

**Figure 4.4 (continued)**



(c)  $DC=2*3899/(3899+6090)= 78.0659\%$

**Figure 4.4 (continued)**



(d)  $DC=2*1858/(1858+2491)= 85.4449\%$

**Figure 4.4: Assessment of filament segmentation**  
Top: Original colored image, Bottom: Assessment image

The ground truth image making of filament containing images is a process even more subjective and difficult than the corresponding one for flocs. Despite so, we have done our best in making our ground truth images as accurate as possible.

The final set of images shows a filament object from the second set and it can be seen that segmentation for the individual detected objects are in fact quite good although sometimes the returned values may seem to be a bit low.

Overall, a visual qualitative assessment clearly suggests that many filament regions have been successfully segmented by the developed algorithm.



The accuracy values from Figure 4.4 are displayed in Table 4.2. From the sets of *a*, *b* and *c* the average accuracy value has been calculated.

**Table 4.2: Dice Coefficient Values for Filament Images**

Image	Accuracy(Dice Coefficient)
a	65.0497%
b	60.4527%
c	78.0659%
Average	67.8561%

#### **4.4 Assessment via Comparisons with non-Digital Imaging Methods**

The first assessment in this section is via a comparison with the laser particle sizing method.

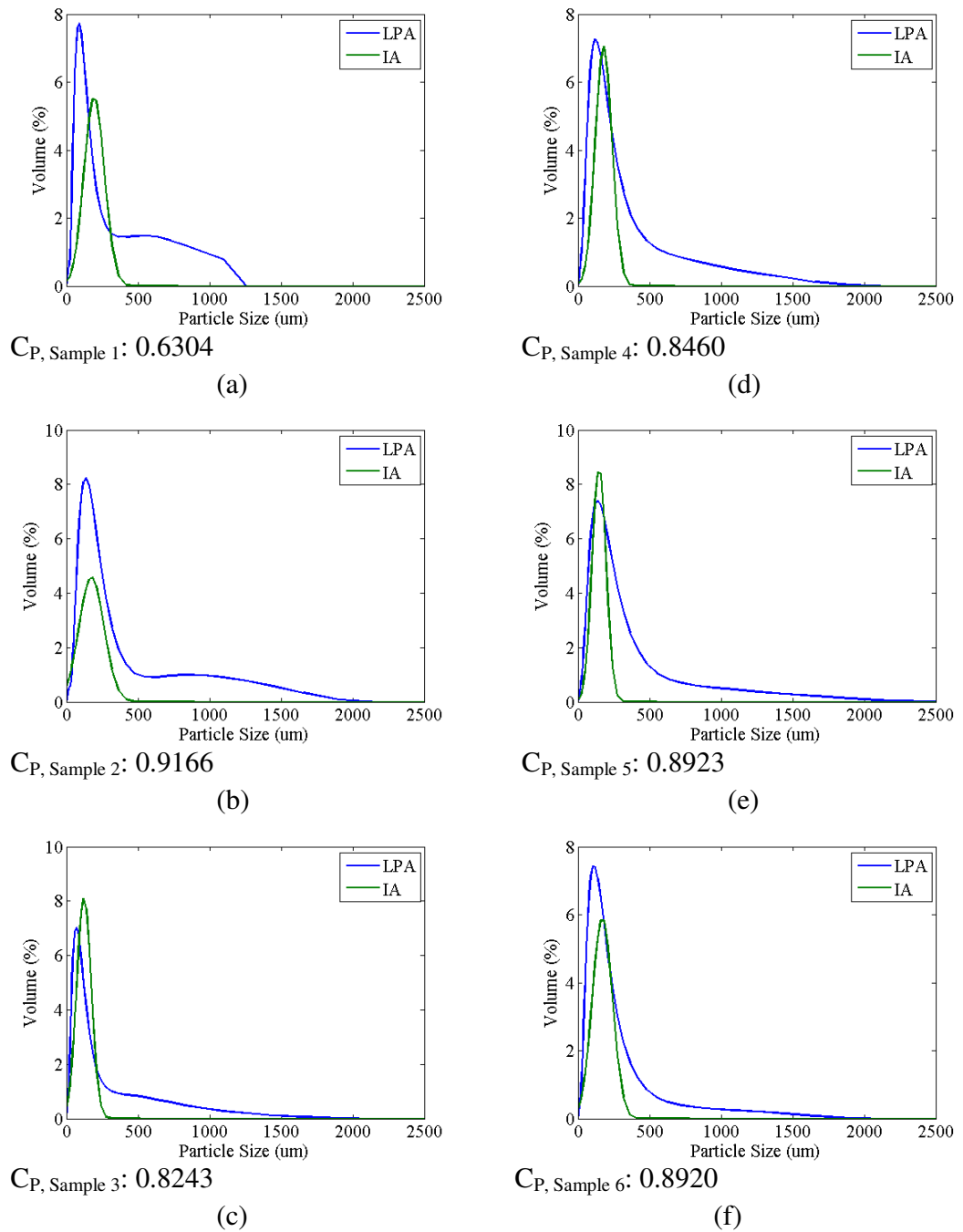


**Figure 4.5: Floc volume percentage vs particle size distribution graphs for 6 samples for digital image analysis and laser particle size analyser methods**

Figure 4.5 shows the distribution of particle size using both methods (LPA: Laser Particle size Analyser; IA: Image Analysis). The correlation coefficient

values from a Pearson's correlation analysis are the values found at the bottom of the individual graphs. The values show the similarity of the two lines plotted on the same graph. The coefficient value itself ranges from 0 to 1, indicating increasing similarity as the value approaches 1. From Figure 4.5, we observe high correlation values for all samples with all samples having a coefficient value larger than 0.8 except for sample 1 only.

For a qualitative assessment, 8 samples have been utilized for graph plotting and the results are seen in Figure 4.6.

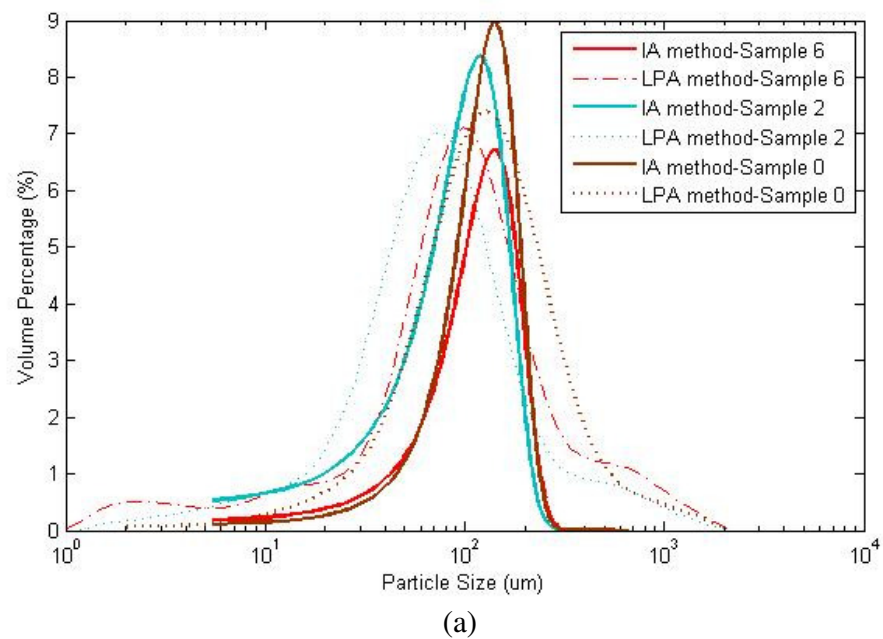
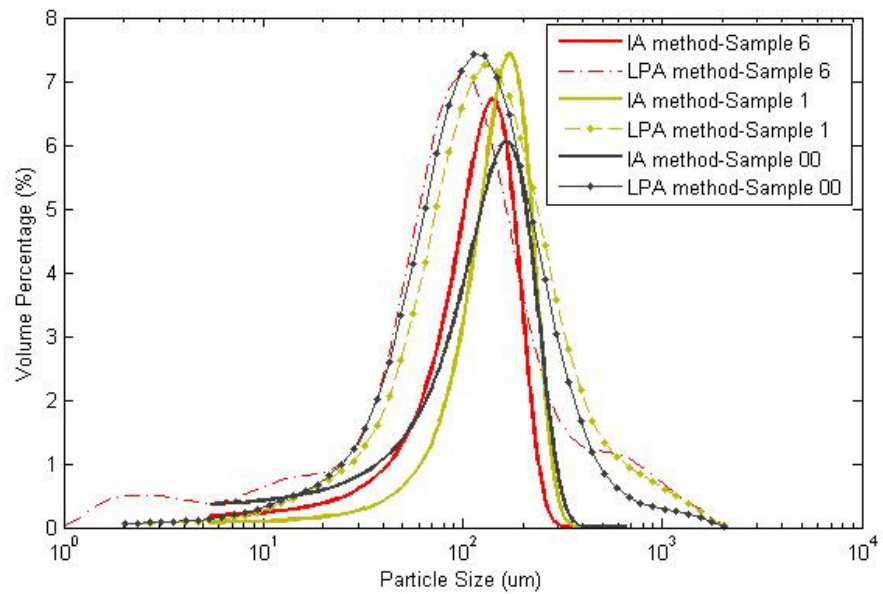
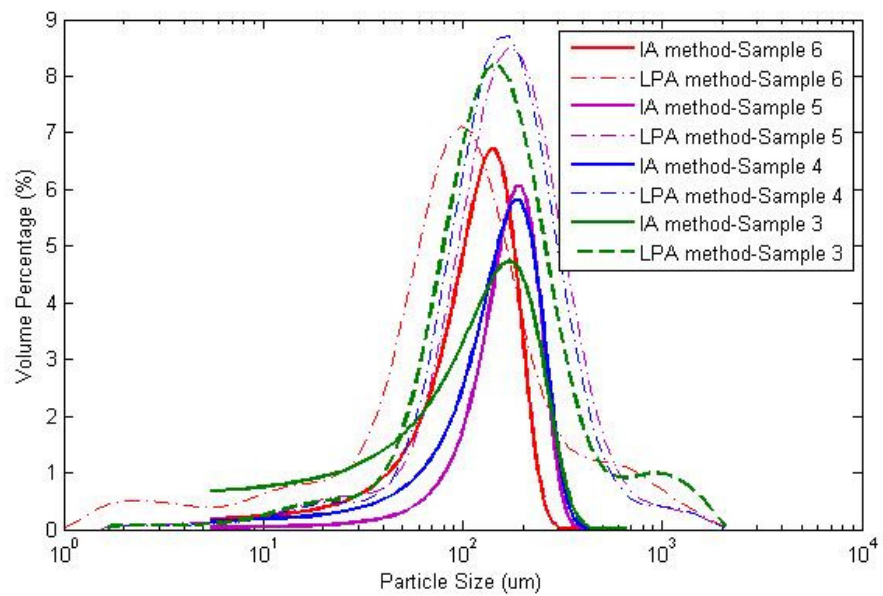


**Figure 4.6 (continues on next page)**



(b)



(c)

**Figure 4.6: Floc volume percentage vs particle size distribution graphs for 8 samples for digital image analysis and laser particle size analyser methods**

For the image analysis (IA) method as shown in Figure 4.6, the volume of the detected floc objects have been calculated by assuming all objects as being spherical in shape, and by using the equivalent diameters of all detected 2D floc objects as diameters of the 3D sphere objects. The equivalent diameter parameter used here is a parameter that specifies for its value the diameter value of a circle with the same area as the region being detected and processed.

The lines from IA method in the graphs of Figure 4.6 are the curve fitted lines via the Gaussian fitting method in Matlab, making the data points fit into multiple peak Gaussian function lines, defined as below:

$$y = \sum_{k=1}^n a_k e^{-\left(\frac{x-b_k}{c_k}\right)^2} \quad (4.1)$$

where a is the amplitude, b is the centroid, c is related to the peak width and n is the number of peaks for fitting ranging from 1 to 8.

The value of n is set to 1, giving only a single peak producing a normal Gaussian shape. The resultant shapes make comparisons with the post-fitted lines from the laser particle size analyser method as provided by the equipment's software more easily done.

Lines from both methods share the same x-axis labeled with the name 'particle size'. For our purpose here, the detected floc objects have been taken to

indicate and represent the particles processes in the laser particle size analyser method considering how the floc objects are the most prominent and big-sized objects in the captured images of our sludge samples.

It is qualitatively observed that line shape similarities of the graphs exist between the digital image analysis method (IA) and the laser particle size analyser (LPA) method. The lines of two methods share the same color if they are of the same sample but are solid for IA method while unconnected for LPA method. In order not to have an overcongested graph, lines from all samples have been divided into 3 groups and plotted separately in a way that makes for optimum ease of comparison.

For peaks in both methods, in the first plot, sample 2 is considerably leftward of sample 6; in the second plot, sample 00 is rightward of sample 1 and sample 1 rightward of sample 6; and finally in the third and last plot, all other samples are towards the right of sample 6.

We can hence, observe qualitatively that the lines from the IA method have agreed in trend with the ones from the LPA method. Combined with the previous quantitative analysis, both qualitative and quantitative analyses have managed to show strong evidence of correlation and similarity in the results of digital imaging method to those of the laser particle sizing method. This supports

our hypothesis that digital imaging may be used as a method in place of laser particle sizing.

Last but not least, it is noted that although the qualitative analysis utilized 8 samples, only 6 samples starting with the label of 'sample 1' in Figure 4.6 are used for all the other analyses of our study due to the fact that filament images have not been satisfactorily captured for the first two samples.

For the next analysis, the results obtained from the tests of TSS and SVI are summarized in Table 4.3.

**Table 4.3: Sludge Volume Index and Total Suspended Solids**

<b>Sample</b>	<b>TSS or MLSS(mg/L)</b>	<b>SVI(mL/g)</b>
1	825	55.76
2	846	48.46
3	425	43.53
4	1002	117.76
5	997	122.37
6	884	139.14

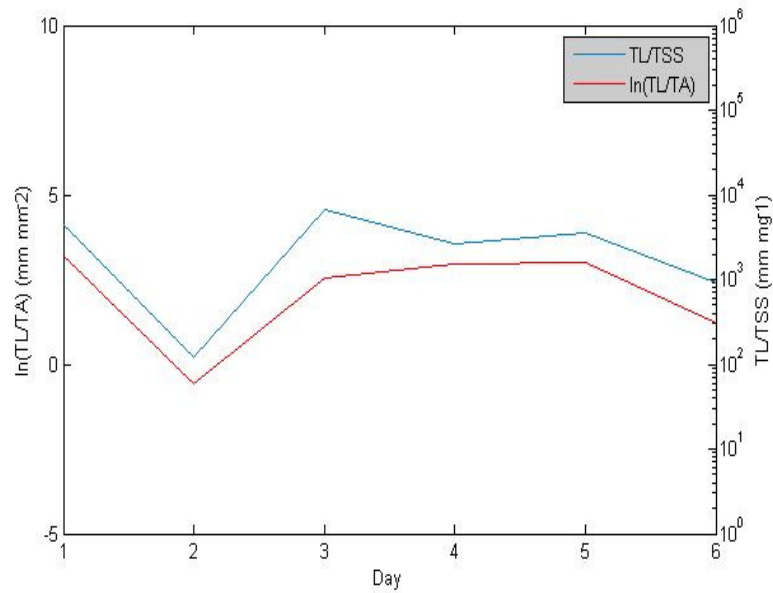


**Figure 4.7: Line graph for IA & TSS using methods across 6 days**  
(TL: Total Length of filaments; TA: Total Area of flocs)

From the work of Mesquita et al. (2011b), when plotted as such as a line plot found in Figure 4.7, the lines from digital imaging methods alone and from physico-chemical methods and digital imaging methods share the same shape. Despite two very different y axis in magnitude and in nature with one being linear with the other one being logarithmic, the extremely high shape similarity from the work of Mesquita et al. (2011b) has been reproduced here for this research. For the plotting of the graph of Figure 4.7, the area values of the filament regions have been used as the length values of the filaments. Considering the case that the filaments are highly thin and threadlike in shape, being naturally low in variability in thickness and also due to the way the algorithm works, the length of filaments and the area of filaments share a linear relationship with each other. Assuming the case that the high correlation observed above holds true for all range of values for



the Total Length variable input, a linear reduction in the Total Length variable values will still produce the same graph with highly correlated line shapes.

Via a comparison with the similar line graphs in the paper by Mesquita et al. (2011b), the condition of the plant as indicated here throughout the samples is seen to be very similar to the line shape and values for the normal condition graph. The shape is very different and distinct from the one of the filamentous bulking graph, giving the same results that the SVI values give, namely that there has been no instance of filamentous bulking in our samples collected. However, the line of the zooglear/ viscous bulking graph which is little differentiated from the one of the normal condition also shows a very high similarity to the line of our graph. By observing the images from our database the possibility of the occurrence of this condition can be ruled out due to the absence of oversized floc-objects that define such a condition.

#### **4.5 Floc Object Morphological Parameter Analysis**

Morphological parameter analysis involving the four parameters of equivalent diameter, roundness, compactness and convexity are done.

All the above morphological parameters except equivalent diameter have values that range from 0 to 1, indicating increasing adherence to the quality of the

parameters themselves as is seen indicated by their names. An explanatory example can be seen in Figure 4.8.

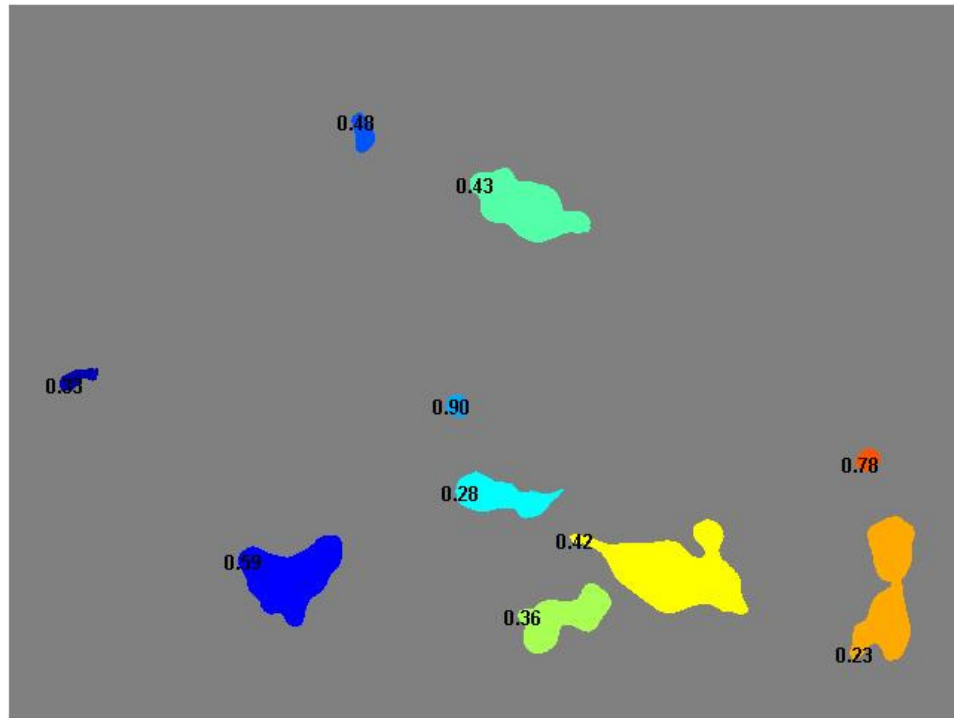


**Figure 4.8: Image with floc objects segmented and respective 'roundness' values labelled**

The Pearson's linear correlation coefficients for floc morphological parameter pairs have been calculated and shown in Table 4.4.

**Table 4.4: Pearson Correlation Coefficients for Sample 1 to Sample 6**

Sample 1- SVI: 55.78				
	ED	Rd	Cm	Cv
ED	1	-0.4750	-0.6018	-0.6393
Rd	-0.4750	1	0.8874	0.7529
Cm	-0.6018	0.8874	1	0.9187
Cv	-0.6393	0.7529	0.9187	1

(a)

Sample 4- SVI: 117.76				
	ED	Rd	Cm	Cv
ED	1	-0.4906	-0.6571	-0.6626
Rd	-0.4906	1	0.8531	0.7271
Cm	-0.6571	0.8531	1	0.9332
Cv	-0.6626	0.7271	0.9332	1

(d)

Sample 2- SVI: 48.46				
	ED	Rd	Cm	Cv
ED	1	-0.4549	-0.6245	-0.6499
Rd	-0.4549	1	0.8404	0.7023
Cm	-0.6245	0.8404	1	0.9251
Cv	-0.6499	0.7023	0.9251	1

(b)

Sample 5- SVI: 122.37				
	ED	Rd	Cm	Cv
ED	1	-0.3956	-0.4786	-0.4814
Rd	-0.3956	1	0.8618	0.7348
Cm	-0.4786	0.8618	1	0.9125
Cv	-0.4814	0.7348	0.9125	1

(e)

Sample 3- SVI: 43.53				
	ED	Rd	Cm	Cv
ED	1	-0.5484	-0.6122	-0.6042
Rd	-0.5484	1	0.8971	0.7314
Cm	-0.6122	0.8971	1	0.9023
Cv	-0.6042	0.7314	0.9023	1

(c)

Sample 6- SVI: 139.14				
	ED	Rd	Cm	Cv
ED	1	-0.5181	-0.7182	-0.7238
Rd	-0.5181	1	0.8388	0.7103
Cm	-0.7182	0.8388	1	0.9282
Cv	-0.7238	0.7103	0.9282	1

(f)

The Pearson's linear correlation coefficients vary from -1 and +1, where -1 corresponds to a perfect negative correlation and +1 corresponds to perfect positive correlation.

From Table 4.4, the values calculated shown do not seem to exhibit clear and regular observable patterns that are correlated with the SVI values.

**Table 4.5: Average Values of Morphological Parameter for Floc Objects Divided into Three Size Classes for Sample 1 to Sample 6**

<b>Sample 1- SVI: 55.78</b>			
SizeClass Ave\	< 75um	>=75um, <150um	>=150um
Numbers	180	235	100
Perc (515)	34.95%	45.63%	19.42%
EqDia	60.8749	105.4973	197.1047
Round.	0.7630	0.6307	0.4785
Compact.	0.8168	0.7335	0.5179
Convexity	0.9718	0.9413	0.8180

(a)

<b>Sample 4- SVI: 117.76</b>			
SizeClass Ave\	< 75um	>=75um, <150um	>=150um
Numbers	174	252	93
Perc (519)	33.53%	48.55%	17.92%
EqDia	58.6674	106.4522	187.3367
Round.	0.7265	0.5726	0.4698
Compact.	0.7926	0.6706	0.4589
Convexity	0.9643	0.9124	0.7862

(d)

<b>Sample 2- SVI: 48.46</b>			
SizeClass Ave\	< 75um	>=75um, <150um	>=150um
Numbers	215	375	109
Perc(699)	30.76%	53.65%	15.59%
EqDia	61.7262	101.9941	195.7167
Round.	0.7350	0.6758	0.4942
Compact.	0.8099	0.7752	0.5362
Convexity	0.9731	0.9574	0.8363

(b)

<b>Sample 5- SVI: 122.37</b>			
SizeClass Ave\	< 75um	>=75um, <150um	>=150um
Numbers	253	451	94
Perc (798)	31.70%	56.52%	11.78%
EqDia	61.2655	104.5754	172.4138
Round.	0.7095	0.6005	0.4842
Compact.	0.7873	0.6996	0.5584
Convexity	0.9656	0.9286	0.8467

(e)

<b>Sample 3- SVI: 43.53</b>			
SizeClass Ave\	< 75um	>=75um, <150um	>=150um
Numbers	652	658	64
Perc(1374)	47.45%	47.89%	4.66%
EqDia	60.4760	100.5163	177.0159
Round.	0.7725	0.6047	0.4111
Compact.	0.8324	0.7092	0.4710
Convexity	0.9728	0.9268	0.7874

(c)

<b>Sample 6- SVI: 139.14</b>			
SizeClass Ave\	< 75um	>=75um, <150um	>=150um
Numbers	417	476	144
Perc(1037)	40.21%	45.90%	13.89%
EqDia	60.3363	105.1724	190.2217
Round.	0.7179	0.5877	0.4335
Compact.	0.7969	0.6776	0.4215
Convexity	0.9667	0.9126	0.7592

(f)

As with the previous tables, the same morphology parameters of equivalent diameter, roundness, compactness and convexity are used, and have their average values calculated for the segmented flocs according 3 size class divisions of small, medium and large. Two clusters/groupings of data have been observed for the data which are the grouping with the background highlighted in

light red and the one in dark green. This pattern agrees with the clustering pattern of the SVI values that can be seen below the tables. The values with light red background are seen to have values consistently larger than those in dark green. In both cases the pattern was stronger for the smaller size classes of small and medium and only slightly weaker for the large size class which is somehow expected due to a less averaging and more outlier-influenced effect due to less objects belonging in this class among other reasons.

The pattern observed persists even when no division of floc objects into size classes is made. This can be seen in Table 4.6.

**Table 4.6: Average Values of Morphological Parameter for Size-Undivided Floc Objects for Sample 1 to Sample 6**

Sample 1- SVI: 55.78	
Numbers	515
EqDia	107.6889
Round.	0.6474
Compact.	0.7207
Convexity	0.9280

(a)

Sample 4- SVI: 117.76	
Numbers	519
EqDia	104.9256
Round.	0.6057
Compact.	0.6736
Convexity	0.9072

(d)

Sample 2- SVI: 48.46	
Numbers	699
EqDia	104.2233
Round.	0.6657
Compact.	0.7486
Convexity	0.9433

(b)

Sample 5- SVI: 122.37	
Numbers	798
EqDia	98.8353
Round.	0.6214
Compact.	0.7108
Convexity	0.9307

(e)

Sample 3- SVI: 43.53	
Numbers	1374
EqDia	85.0794
Round.	0.6753
Compact.	0.7565
Convexity	0.9421

(c)

Sample 6- SVI: 139.14	
Numbers	1037
EqDia	98.9529
Round.	0.6186
Compact.	0.6900
Convexity	0.9130

(f)

Size class division allows for more comparison of data values for more proof of pattern existence as well as ideally a more pronounced trend in the medium size class. It is observed here that the pattern observed from the undivided tables is similarly as strong as the one in the divided medium class. This proves the strength of the pattern identified, allowing for a simple size-undivided morphological parameter analysis to suffice for state identification of the water plant. However, it is to be seen that as more samples are utilized, the

agreeing trends in multiple divisions would prove to be more useful as more indication strength.

In Figure 4.9 the data of Table 4.6 are displayed in chart forms for another observation of the trend discussed before. From Figure 4.10 to Figure 4.12 the data of Table 4.5 are used.

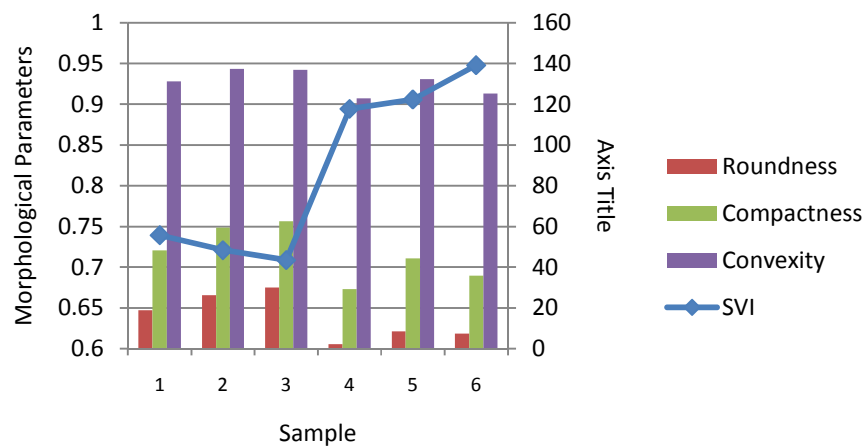


**Figure 4.9: Chart of morphological parameter and SVI values for 6 samples**  
(Left axis: bar chart; Right axis: line chart)

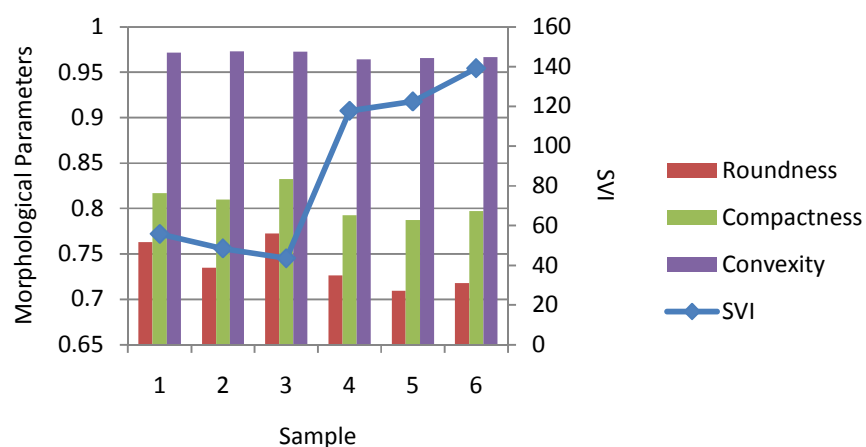


**Figure 4.10: Chart of morphological parameter and SVI values for small objects for 6 samples**  
(Left axis: bar chart; Right axis: line chart)

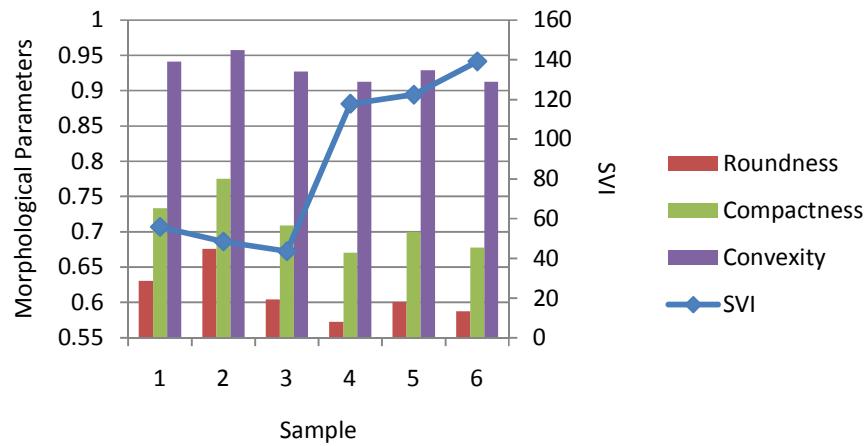


**Figure 4.11: Chart of morphological parameter and SVI values for medium objects for 6 samples (Left axis: bar chart; Right axis: line chart)**

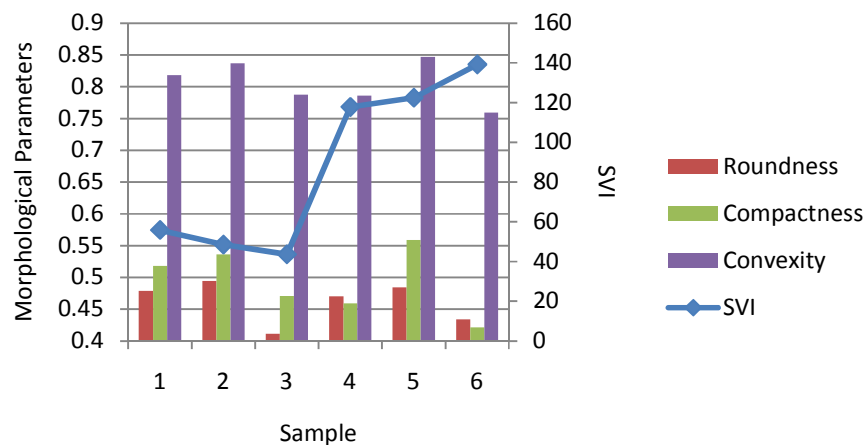
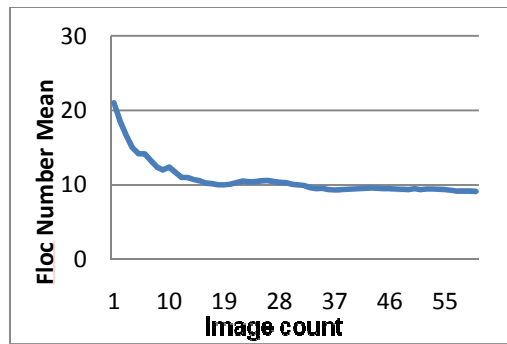


**Figure 4.12: Chart of morphological parameter and SVI values for large objects for 6 samples (Left axis: bar chart; Right axis: line chart)**

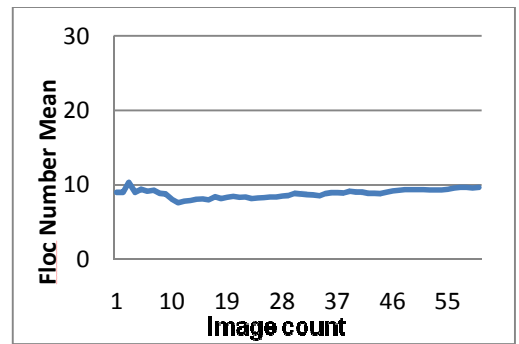
#### 4.6 Study on the Appropriate Number of Images for Processing

The distribution line graphs for the number of images processed by the algorithm versus the calculated mean number of flocs per image have been plotted and are shown in Figure 4.13.

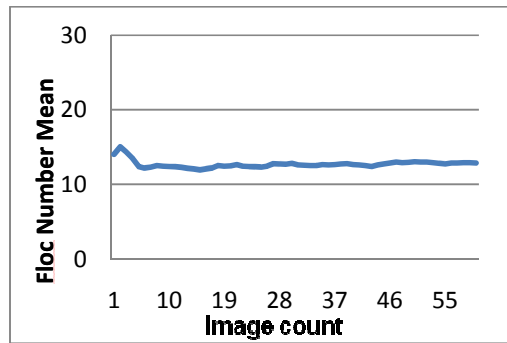




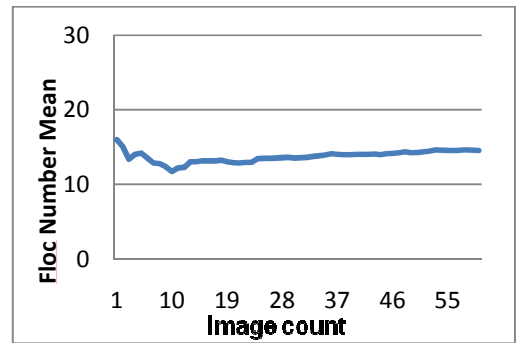
(a)



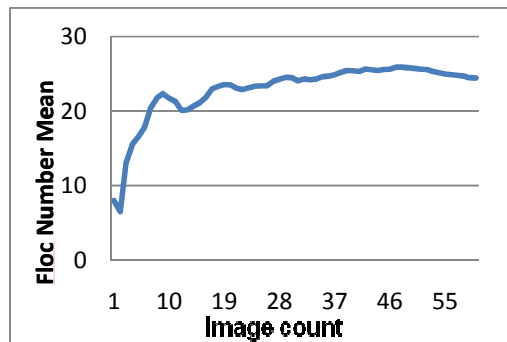
(d)



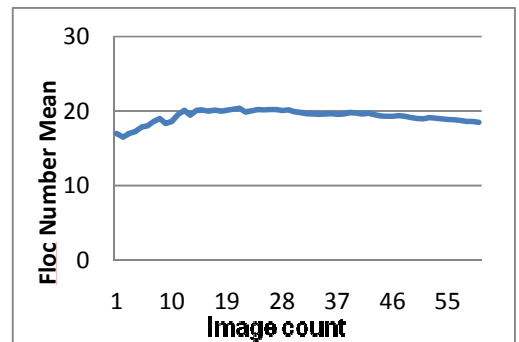
(b)



(e)



(c)



(f)

**Figure 4.13: Number of images processed vs the mean number of flocs per image distribution graph over 6 samples (a-f: sample 1 to sample 6)**

A total of 60 images have been processed for each day/sample for Figure 4.13. It is observed here that for all samples, the mean number of flocs found per

image parameter has its values stabilized at approximately/around the mark of 20 images being processed by the algorithm. It can be seen that a sufficient number of images for floc object processing has been used for our research seeing as the mean number of the floc objects per image stabilizes at around the 20-images-processed mark.

## CHAPTER 5

### CONCLUSIONS AND FUTURE DIRECTIONS

#### 5.1 Overview

In the research documented by this dissertation algorithms have been successfully developed for the segmentation of the floc and filament objects found in sludge of the activated sludge waste water treatment process (WWTP) plants. The algorithms developed are background illumination invariant and give good segmentation results. An average Dice coefficient value of 71.85% has been obtained for the floc segmentation algorithm for processing the samples while for the filament segmentation algorithm a value of 67.86% has been obtained.

Correlation between the results of digital imaging methods and the results of more established physico-chemical methods are also seen to be existent and high in value in quantitative analysis. Similar line shapes from digital imaging method against laser particle sizing method graph produced Pearson's correlation coefficient values larger than 0.8 in 5 of 6 samples processed indicating high similarity. The highly matching line shape is also seen in the graph of image analysis against total suspended solids plus image analysis method. In morphological parameter analysis, when analysed individually, the morphological

parameter values considered in the dissertation for each floc object did not seem to be correlated with each other in patterns that change according to the SVI values; however, when analysed as whole by taking the average values for all objects first divided into 3 size class division and then undivided, data trends that correlated well to the SVI index values have been observed.

## **5.2 Future Work Recommendations**

Future work should consider and analyse more morphological parameters such as fractal dimension for the discovery of a highly probable similar correlation pattern in existence.

Lab-scale set up that allows for control of the tank conditions is also highly useful to allow for a controllable and wider range of SVI values which in the current study is being determined by the state of the wastewater treatment plant being visited for sludge sample collection.

To gain clearer microscopic visualizations of not only the floc and filament objects but also of other microscopic organisms, sample staining procedures may be considered and conducted in the image acquisition procedures of future studies.

## REFERENCES

Amaral, A.L. et al., 1999. Semi-automated recognition of protozoa by image analysis. *Biotechnolol. Tech.* 13: 111-118

Amaral, A.L., 2003. *Image analysis in biotechnological processes: Applications to wastewater treatment*. Ph.D. Thesis, University of Minho, Braga, Portugal.

Amaral, A. L., & Ferreira, E. C., 2005. Activated sludge monitoring of a wastewater treatment plant using image analysis and partial least squares regression. *Analytica Chimica Acta*, 544(1), 246-253.

Asano, T., Smith, R.G. and Tchobanoglous G., 1985. *Municipal wastewater: Treatment and reclaimed water characteristics. Irrigation with Reclaimed Municipal Wastewater - A Guidance Manual*, G.S. Pettygrove and T. Asano (eds). Lewis Publishers Inc., Chelsea, Mississippi

Bengtson, H. and Malburg, S., 2011a. *Biological Wastewater Treatment Systems for Removal of Biochemical Oxygen Demand* [Online]. Available at <http://www.brighthub.com/environment/science-environmental/articles/66158.aspx> [Accessed: 1 February 2015].

Bengtson, H. and Malburg, S., 2011b. *Variations in Activated Sludge Wastewater Treatment Systems* [Online]. Available at <http://www.brighthub.com/environment/science-environmental/articles/66157.aspx> [Accessed: 1 February 2015].

Bengston, H. and Stonecypher, L., 2013. *The History of Activated Sludge* [Online]. Available at: <http://www.brighthubengineering.com/geotechnical-engineering/77786-the-history-of-activated-sludge/> [Accessed: 1 February 2015]

Contreras, E. M., Giannuzzi, L., & Zaritzky, N. E., 2004. Use of image analysis in the study of competition between filamentous and non-filamentous bacteria. *Water research*, 38(11), 2621-2630.

Dagot, C. et al., 2001. Use of image analysis and rheological studies for the control of settleability of filamentous bacteria: application in SBR reactor. *Water Sci. Technol.* 43:27-33.

Da Motta, M., Pons, M.N. and Roche, N., 2001a. Automated monitoring of activated sludge in a pilot plant using image analysis. *Water Sci. Technol.* 43: 91-96.

Da Motta, M., Pons, M. N., Roche, N., & Vivier, H., 2001b. Characterisation of activated sludge by automated image analysis. *Biochemical Engineering Journal*, 9(3), 165-173.

Da Motta M., Amaral L.P., Casellas M., Pons M.N., Dagot C., Roche N., Ferreira E.C., Vivier H., 2002. Characterisation of activated sludge by automated image analysis: validation on full-scale plants. *IFAC Computer Applications in Biotechnology*, Québec City, Canada.

Gins, G., Smets, I. V., Jenne, R., Van Impe, J. F., 2005. Activated Sludge Image Analysis Data Classification: An LS-SVM Approach. In *Proceedings of the 16th IFAC World Congress, DVD-ROM, 6p, 16th IFAC World Congress, Prague*.

Gonzalez, R. C., Woods, R. E and Eddins, S.L., 2009. *Digital Image Processing Using MATLAB®* Second Edition: Gatesmark Publishing.

Grady, C.P.L., Daigger, G.T. and Lim, H.C., 1999. *Biological Wastewater Treatment*, 2nd Edition, New York, NY: Marcel Dekker, Inc.

Grijpspeerd, K., & Verstraete, W., 1997. Image analysis to estimate the settleability and concentration of activated sludge. *Water Research*, 31(5), 1126-1134.

Heine, W., Sekoulov, I., Burkhardt, H., Begen, L., Behrendt, J., 2000. Bulking Sludge Observation by Microscopic Observation and Mechanical Treatment. *Tagungsband der 12. Fachtagung zur Weitergehenden Abwasserreinigung als Beitrag zum Schutz von Nord- und Ostsee Travemünde, Germany.*

Heine, W., Sekoulov, I., Burkhardt, H., Begen, L. and Behrendt, J., 2001. Early warning-system for operation-failures in biological stages of WWTPs by on-line image analysis. *IWA Conference in Berlin*, 15-19 October.

Jenkins, D., Richard, M.G., Daigger, G., 2003. *Manual on the Causes and Control of Activated Sludge Bulking, Foaming and Other Solids Separation Problems*: Lewis Publishing.

Jenne, R., Cenens, C., Geeraerd, A. H. and Van Impe, J. F., 2002. Towards on-line quantification of flocs and filaments by image analysis. *Biotechnology Letters* 24: 931-935.

Jenné R., Banadda E. N., Philips N., Van Impe J. F., 2003. Image Analysis as a Monitoring Tool for Activated Sludge Properties in Lab-Scale Installations. *Journal of Environmental Science and Health, Part A* Vol. 38, Iss. 10.

Jin, B., Wilén, B. M., & Lant, P., 2004. Impacts of morphological, physical and chemical properties of sludge flocs on dewaterability of activated sludge. *Chemical Engineering Journal*, 98(1), 115-126.

Larptansuphaphol, T., & Jitjumroonchokchai, P., 2010. Investigation on filamentous micro-organisms in sludge foaming from pulp & paper mill wastewater treatment plant.

Liwarska-Bizukojc, E., 2005. Application of image analysis techniques in activated sludge wastewater treatment processes. *Biotechnology Letters* 27: 1427-1433, DOI 10.1007/s10529-005-1303-2.

- Liwerska-Bizukojc, E. and Bizukojc, M, 2005. Digital image analysis to estimate the influence of sodium dodecyl sulphate on activated sludge flocs. *Proc. Biochem.* 40: 2067-2072.
- McAndrew, A., 2004. *An Introduction to Digital Image Processing with Matlab: Course Technology.*
- Mesquita, D.P., Dias, O., Dias, A.M.A., Amaral, A.L. and Ferreira, E.C., 2008. Evaluation of activated sludge systems by image analysis procedures. *Proceedings of the International Symposium on Sanitary and Environmental Engineering: SIDISA 08 [CD-ROM]*, Florence, Italy, 24-27 June, pp: 1-8.
- Mesquita, D. P., Dias, O., Dias, A. M. A., Amaral, A. L., & Ferreira, E. C., 2009. Correlation between sludge settling ability and image analysis information using partial least squares. *Analytica chimica acta*, 642(1), 94-101.
- Mesquita, D. P., Dias, O., Amaral, A. L., & Ferreira, E. C., 2009. Monitoring of activated sludge settling ability through image analysis: validation on full-scale wastewater treatment plants. *Bioprocess and biosystems engineering*, 32(3), 361-367.
- Mesquita, D.P., Amaral A. L. and Ferreira E. C., 2010. Disturbances detection in activated sludge systems, *Semana de Engenharia*.
- Mesquita, D. P., Dias, O., Amaral, A. L., & Ferreira, E. C., 2010. A Comparison between bright field and phase-contrast image analysis techniques in activated sludge morphological characterization. *Microscopy and Microanalysis*, 16(02), 166-174.
- Mesquita, D. P., Amaral, A. L., & Ferreira, E. C., 2011a. Characterization of activated sludge abnormalities by image analysis and chemometric techniques. *Analytica chimica acta*, 705(1), 235-242.



Mesquita, D. P., Amaral, A. L., & Ferreira, E. C., 2011b. Identifying different types of bulking in an activated sludge system through quantitative image analysis. *Chemosphere*, 85(4), 643-652.

Mesquita, D.P., Amaral A. L. and Ferreira E. C., 2011c. Quantitative image analysis for sludge volume index and total suspended solids prediction in activated sludge system disturbances. *Book of Abstracts of the 11th International Chemical and Biological Engineering Conference, Lisbon, Portugal, 5-7 September*

Niblack, W., 1986. *An Introduction to Digital Image Processing*. Englewood Cliffs: Prentice-Hall.

Perez Y. G., Leite S. G .F. and Coelho M. A. Z., 2006. Activated sludge morphology characterization through an image analysis procedure. *Brazilian Journal of Chemical Engineering* Vol. 23, No. 03, pp. 319 - 330, July – September. ISSN 0104-6632.

Sikora, M., & Smolka, B., 2001. Feature analysis of activated sludge based on microscopic images. In *Electrical and Computer Engineering, 2001. Canadian Conference on* (Vol. 2, pp. 1309-1314). IEEE.

Tchobanoglous, G., Burton, F.L. and Stensel, H.D., 2002. *Wastewater Engineering Treatment and Reuse*, 4th Edition: McGraw-Hill Science/Engineering/Math.

Toprak, H., 2006. *Sedimentation Facilities for the Activated-Sludge Process* [Online]. Available at: <http://web.deu.edu.tr/atiksu/ana52/ani4091.html> [Accessed: 1 February 2015]

Vesilind, P.A. and Morgan, S.M., 2004. *Introduction to Environmental Engineering*, 2nd Edition: CRC Press.

Waite, T.D., Guan, J. and Amal, R., 1998. Rapid determination of bacterial assemblage structure: implications to process optimisation in wastewater

treatment. In: E. Hoffmann and H. Odegaard (eds). *Chemical Water and Wastewater Treatment V*. Berlin: Springer-Verlag, 269–283.

Wilén, B. M., Jin, B., & Lant, P., 2003. Impacts of structural characteristics on activated sludge floc stability. *Water research*, 37(15), 3632-3645.

Wilén, B. M., Onuki, M., Hermansson, M., Lumley, D., & Mino, T., 2008. Microbial community structure in activated sludge floc analysed by fluorescence in situ hybridization and its relation to floc stability. *Water research*, 42(8), 2300-2308.

Yu, R.F., Chen, H.W. and Cheng, W.P., 2009. Simultaneously monitoring the particle size distribution, morphology and suspended solids concentration in wastewater applying digital image analysis (DIA). *Environ Monit Assess* 148:19-26.

Zou, K.H., Warfield, S.K., Bharatha, A., Tempany, C.M., Kaus, M.R., Haker, S. J., Wells, W.M., Jolesz, F.A., & Kikinis, R., 2004. Statistical validation of image segmentation quality based on a spatial overlap index 1: Scientific reports. *Academic radiology*, 11(2), 178-189.

**Credits:**

Gonzalez, R. C., Woods, R. E and Eddins, S.L., 2009. *Digital Image Processing Using MATLAB®* Second Edition: Gatesmark Publishing.

Figure 1.3 from:

<http://www.brighthub.com/environment/science-environmental/articles/66158.aspx>

Figure 1.4 to Figure 1.6 from:

<http://web.deu.edu.tr/atiksu/ana52/ani4091.html>

Figure 1.7 from:

<http://particle.dk/methods-analytical-laboratory/particle-size-by-laser-diffraction/laser-diffraction-theory/>

Contents of Table 1.1 from <http://www.wrights-trainingsite.com/ActSlud1onb.html>

**Relevant Publications by Author:**

Lee X.Y., Nisar H., Yeap K. H., Ng C. A., Malik A. S., 2014. Morphological Analysis of Activated Sludge Flocs and Filaments. *2014 IEEE International Instrumentation and Measurement Technology Conference*, May 12-15, Montevideo, Uruguay.

Lee X.Y., Nisar H., Yeap K. H., 2013. An Approach for Segmentation and Quantification of Activated Sludge Floc Blobs. *Advanced Science Letters*, July 2013.

Nisar H., Lee X. Y., Yeap K. H., Yap V. V., Soh C. S., 2012. Application of Imaging Techniques for Monitoring Flocs in Activated Sludge. *Intl. Conf. on Biomedical Engineering*, Malaysia, Feb 27-28.

Khan, M. B., Lee, X. Y., Nisar, H., Ng, C. A., Yeap, K. H., & Malik, A. S., 2015. Digital Image Processing and Analysis for Activated Sludge Wastewater Treatment. In: *Signal and Image Analysis for Biomedical and Life Sciences* (pp. 227-248). Springer International Publishing.

## APPENDIX A

### Matlab Programming Code

```
%% Floc Algo

qv1 = imread('snap-01.jpg');qv2 = imread('snap-02.jpg');
qv3 = imread('snap-03.jpg');qv4 = imread('snap-04.jpg');
qv5 = imread('snap-05.jpg'); %And more...
qv = {qv1,qv2,qv3,qv4,qv5,qv6,qv7,...
      qv8,qv9,qv10,qv11,qv12,qv13,qv14,...
      qv15,qv16,qv17,qv18,qv19,qv20,qv21,...
      qv22,qv23,qv24,qv25,qv26,qv27,qv28};
      qv29,qv30,qv31,qv32,qv33,qv34,qv35,...
      qv36,qv37,qv38,qv39,qv40,qv41,qv42};
qvii = {qv43,qv44,qv45,qv46,qv47,qv48,qv49, ...
        qv50,qv51,qv52,qv53,qv54,qv55,qv56, ...
        qv57,qv58,qv59,qv60,qv61,qv62,qv63, ...
        qv64,qv65,qv66,qv67,qv68,qv69,qv70};
        qv71,qv72,qv73,qv74,qv75,qv76,qv77, ...
        qv78,qv79,qv80,qv81,qv82,qv83,qv84, ...
        qv85,qv86,qv87,qv88,qv89,qv90,qv91};

for x=1:35
    hmin0{1,x} = imhmin(qv{1,x},50);
    % figure,imshow(hmin0{1,x});
end
for x=36:60
    hmin0{1,x} = imhmin(qvii{1,x-35},50);
    % figure,imshow(hmin0{1,x});
end
```

```

for x=1:60
    meddd{1,x} = medfilt2(hmin0{1,x},[25 25]);
    % figure,imshow(meddd{1,x},'Border','tight');
end

h = fspecial('average', [50 50]);
for x=1:60
    averaged{1,x} = imfilter(meddd{1,x},h,'replicate');
end

for x=1:35
    nb8{1,x}=im2uint8(niblack(averaged{1,x}, [500 500], -0.2, 5));
end
for x=36:60
    nb8ii{1,x-35}=im2uint8(niblack(averaged{1,x}, [500 500], -0.2, 5));
end

for x=36:60
    borderclred{1,x}= ~imclearborder( ~nb8ii{1,x-35});end
for x=1:35
    borderclred{1,x}= ~imclearborder( ~nb8{1,x});end

for x=1:60
    aroped{1,x}=bwareaopen (~borderclred{1,x},2457);%4915
    % % figure,imshow(~aroped{1,x},'Border','tight');
end

%% floc analysis
clear flcareacell flcroundnesscell flcformfactorcell flcEqdiacell flcconvexitycell
flcvolume EdRdFfCv;
flc1EqDia=0; flc1Roundness=0; flc1FormFactor=0; flc1Convexity=0; flc1Denom=0;
flc2EqDia=0; flc2Roundness=0; flc2FormFactor=0; flc2Convexity=0; flc2Denom=0;
flc3EqDia=0; flc3Roundness=0; flc3FormFactor=0; flc3Convexity=0; flc3Denom=0;

```

```

fferror=0;
kforcorr=1;
catobjs=0;
numflocacc=0;
allimg_volumetotal=0;

allimg_flocarea=0;

for y=1:55
flcEdctg(1,y)=0;
end
j=1;
for x=1:55
CC = bwconncomp(aropedGT2{1,x});
Lfloc = labelmatrix(CC);
sfl
=regionprops(aropedGT2{1,x},'Area','MajorAxisLength','Perimeter','PixelList','EquivalentArea','ConvexArea');

numflocacc=numflocacc+CC.NumObjects;
meanflocnum(1,j)=numflocacc/j;
j=j+1;

for k=1:CC.NumObjects
flcareacell{1,x}(1,k)=sfl(k).Area;

roundness(k) = 4*(sfl(k).Area)/pi/((sfl(k).MajorAxisLength)^2);
flcroundnesscell{1,x}(1,k)=roundness(k);

formfactor(k)= 4*pi* (sfl(k).Area)/ ((sfl(k).Perimeter)^2);
flcformfactorcell{1,x}(1,k)=formfactor(k);

```

```

convexity(k)=sfl(k).Area/sfl(k).ConvexArea;
flcconvexitycell{1,x}(1,k)=convexity(k);

flcEqdiacell{1,x}(1,k)= sfl(k).EquivDiameter *0.839;

flcvolume{1,x}(1,k)= 4/3*pi*(.5*flcEqdiacell{1,x}(1,k))^3;
% flcsurfacearea{1,x}(1,k)= 4*pi*(.5*flcEqdiacell{1,x}(1,k))^2;

allimg_volumetotal=allimg_volumetotal+flcvolume{1,x}(1,k);
% allimg_surfacearea=allimg_surfacearea+flcsurfacearea{1,x}(1,k);

allimg_flocarea= allimg_flocarea+sfl(k).Area;%*0.839*0.839*2;

if sfl(k).EquivDiameter < (75/0.839)
    flc1EqDia=flc1EqDia+sfl(k).EquivDiameter *0.839;
    flc1Roundness=flc1Roundness+roundness(k);
    flc1FormFactor=flc1FormFactor+formfactor(k);
    flc1Convexity=flc1Convexity+convexity(k);
    flc1Denom=flc1Denom+1;
else if sfl(k).EquivDiameter < (150/0.839)
    flc2EqDia=flc2EqDia+sfl(k).EquivDiameter *0.839;
    flc2Roundness=flc2Roundness+roundness(k);
    flc2FormFactor=flc2FormFactor+formfactor(k);
    flc2Convexity=flc2Convexity+convexity(k);
    flc2Denom=flc2Denom+1;
else
    flc3EqDia=flc3EqDia+sfl(k).EquivDiameter *0.839;
    flc3Roundness=flc3Roundness+roundness(k);
    flc3FormFactor=flc3FormFactor+formfactor(k);
    flc3Convexity=flc3Convexity+convexity(k);
    flc3Denom=flc3Denom+1;
end
end
end

```

```

if formfactor(k)>1
    ffmorethan1 { 1,x } (1,k)=formfactor(k);
    fferror=fferror+1;
end
EdRdFfCv(kforcorr,1)=sfl(k).EquivDiameter;
EdRdFfCv(kforcorr,2)=roundness(k);
EdRdFfCv(kforcorr,3)=formfactor(k);
EdRdFfCv(kforcorr,4)=convexity(k);
kforcorr=kforcorr+1;

z=0;
y=1;
while catobjjs ~=(kforcorr)
    if flcEqdiacell { 1,x } (1,k)< 60+z
        flcEdctg(1,y)=flcEdctg(1,y)+1;           %plotting in absolute numbers
        catobjjs=catobjjs+1;
    else
        z=z+10;y=y+1;
    end
end
end

end
end
rho=corr(EdRdFfCv);
flc1EqDia=flc1EqDia/flc1Denom;      flc1Roundness=flc1Roundness/flc1Denom;
flc1FormFactor=flc1FormFactor/flc1Denom;
flc1Convexity=flc1Convexity/flc1Denom;
flc2EqDia=flc2EqDia/flc2Denom;      flc2Roundness=flc2Roundness/flc2Denom;
flc2FormFactor=flc2FormFactor/flc2Denom;
flc2Convexity=flc2Convexity/flc2Denom;

```



```

flc3EqDia=flc3EqDia/flc3Denom;      flc3Roundness=flc3Roundness/flc3Denom;
flc3FormFactor=flc3FormFactor/flc3Denom;
flc3Convexity=flc3Convexity/flc3Denom;

%% floc analysis ii
clear diadenom plotdia plotpercentvolume plotcumpercentvolume plotpercentnumber
plotcumpercentnumber plotrd plotff plotcv plotrdpercnumber;
clear plotffpercnumber plotcvpercnumber
kforcorr=0;

for z=1:60
    diadenom(1,z)= 0;
    plotdia(1,z)=0;
    plotpercentvolume(1,z)=0;
    plotcumpercentvolume(1,z)=0;
%    plotpercentsurfarea(1,z)=0;
%    plotcumpercentsurfarea(1,z)=0;
    plotpercentnumber(1,z)=0;
    plotcumpercentnumber(1,z)=0;
end
for y=1:10

    plotrd(1,y)=-0.05+y*0.1;

    plotff(1,y)=-0.05+y*0.1;

    plotcv(1,y)=-0.05+y*0.1;

    plotrdpercnumber(1,y)=0;
    plotffpercnumber(1,y)=0;
    plotcvpercnumber(1,y)=0;
end
i=0;

```

```

for x=1:55

    [Lfloc,numfloc]=bwlabel(aropedGT2{1,x});

    for k=1:numfloc

        objincat=0;
        z=0;
        y=1;

        while objincat ~=1
            if flcEqdiacell{1,x}(1,k)< 40+z
                diadenom(1,y)=diadenom(1,y)+1;
                plotdia(1,y)=plotdia(1,y)+flcEqdiacell {1,x}(1,k);
                plotpercentvolume(1,y)=plotpercentvolume(1,y)+flcvolume
{1,x}(1,k)/allimg_volumetotal*100;
                %
                plotpercentfarea(1,y)=plotpercentfarea(1,y)+flcfacingarea{1,x}(1,k)/allimg_facingare
a*100;
                %
                plotpercentsurfarea(1,y)=plotpercentsurfarea(1,y)+flcsurfacearea{1,x}(1,k)/allimg_su
rfacearea*100;
                plotpercentnumber(1,y)=plotpercentnumber(1,y)+1/numflocacc*100;

                objincat=1;
            else
                z=z+10;y=y+1;
            end

        end

        objincat=0;
    end
end

```

```

z=0;
y=1;
while objjincat ~=1
if flcroundnesscell{1,x}(1,k)<0.1+z %&& flcEqdiacell{1,x}(1,k)>=100
    plotrdpercnumber(1,y)=plotrdpercnumber(1,y)+1/numflocacc*100;

    objjincat=1;
else %if flcEqdiacell{1,x}(1,k)>=100
    z=z+.1;y=y+1;%end
end
% if flcEqdiacell{1,x}(1,k)<100
%     objjincat=1;
% end
end
objjincat=0;
z=0;
y=1;
while objjincat ~=1
if flcformfactorcell{1,x}(1,k)<0.1+z
    plotffpercnumber(1,y)=plotffpercnumber(1,y)+1/numflocacc*100;

    objjincat=1;
else
    z=z+.1;y=y+1;
end
end
objjincat=0;
z=0;
y=1;
while objjincat ~=1
if flcconvexitycell{1,x}(1,k)<0.1+z
    plotcvpercnumber(1,y)=plotcvpercnumber(1,y)+1/numflocacc*100;

```

```

        objincat=1;
    else
        z=z+.1;y=y+1;
    end

end

end

end

end

for y=1:60
    if (y~=1)
        plotcumpercentvolume(1,y)=plotcumpercentvolume(1,y-1)+
plotpercentvolume(1,y);
        % %          plotcumpercentsurfarea(1,y)=plotcumpercentsurfarea(1,y-1)+
plotpercentsurfarea(1,y);
        plotcumpercentnumber(1,y)=plotcumpercentnumber(1,y-
1)+plotpercentnumber(1,y);
    else
        plotcumpercentvolume(1,y)=0+ plotpercentvolume(1,y);
        % %          plotcumpercentsurfarea(1,y)=0+plotpercentsurfarea(1,y);
        plotcumpercentnumber(1,y)=0+plotpercentnumber(1,y);
    end

    if plotdia(1,y)==0
        plotdia(1,y)=25+y*10;
    end

    if diadenom(1,y)==0
        diadenom(1,y)=1;
    end
end
end

```

```

for z=1:60
    plotdia(1,z)= plotdia(1,z)/diadenom(1,z);
end

%% filament algo

hmin0=cell(1,91);
for x=[64:91] %1:4 5:14 15:35 1:21 22:42 43:63
% figure,imshow(qv{1,x},'border','tight');
hmin0{1,x} = imhmin(qvii{1,x-42},30); %50
end
clear qvii
% figure,imshow(hmin0{1,x});

meddd=cell(1,91);
erod=cell(1,91);
binary=cell(1,91);
for x=[64:91] %1:4 5:14 15:35 1:21 22:42 43:63
meddd{1,x} = medfilt2(hmin0{1,x},[25 25]); %then to erod or to averaged

erod{1,x} = imerode(meddd{1,x},(strel('disk',10)) );
% figure,imshow(erod{1,x});
add{1,x}=imadd( (255-erod{1,x} ),hmin0{1,x});
binary{1,x}=im2bw(add{1,x},graythresh(add{1,x})); % method followed by
HoughTransform
% figure,imshow(binary{1,x},'border','tight');
end

h = fspecial('average', [50 50]);
averaged = cell(1,42);
for x=[22:42]%1:4 5:14 15:35 1:21 22:42
averaged{1,x} = imfilter(meddd{1,x},h,'replicate');

```

```

% figure,imshow(averaged{1,x});
end;
clear meddd
nb8 = cell(1,42);
for x=[22:42]%1:4 5:14 15:35 1:21 22:42
nb8{1,x}=im2bw(niblack(averaged{1,x}, [500 500], -0.2, 5)); %im2uint8
% figure,imshow(nb8{1,x},'Border','tight');
end;
dilatnb8 = cell(1,42);
addbin = cell(1,42);
for x=[22:42]%1:4 5:14 1:21 22:42
dilatnb8{1,x}=imdilate(~nb8{1,x},(strel('disk',25)) );%10(old)
% figure,imshow(~dilatnb8{1,x},'Border','tight');

addbin{1,x}=or(binary{1,x},dilatnb8{1,x});
% figure,imshow(binary{1,x},'border','tight');
% figure,imshow(addbin{1,x},'Border','tight');
end

Hlines=cell(1,91);
for x=[64:91] %1:4 5:14 15:35 1:21 22:42 43:59

[Houghmatrix, theta, rho] = hough( ~addbin{1,x});

Hpeaks = houghpeaks(Houghmatrix, 1000,'threshold',0);

Hlines{1,x} = houghlines(~addbin{1,x}, theta, rho, Hpeaks);

figure,imshow(addbin{1,x} ,'Border','tight');
figure, imshow(addbin{1,x} ,'Border','tight'), hold on

for k = 1:length(Hlines{1,x})

```

```

xy = [Hlines{1,x}(k).point1; Hlines{1,x}(k).point2];
plot(xy(:,1),xy(:,2),'-', 'LineWidth',1,'Color','blue');
%%%% Plot beginnings and ends of lines
%plot(xy(1,1),xy(1,2),'-s','LineWidth',1,'Color','yellow');
%plot(xy(2,1),xy(2,2),'-s','LineWidth',1,'Color','red');
end

if x==1 ;export_fig test1.png -native
elseif x==2 ;export_fig test2.png -native
elseif x==3 ;export_fig test3.png -native
elseif x==4 ;export_fig test4.png -native
%
elseif x==5 ;export_fig test5.png -native
elseif x==6 ;export_fig test6.png -native
elseif x==7 ;export_fig test7.png -native
elseif x==8 ;export_fig test8.png -native
elseif x==9 ;export_fig test9.png -native
elseif x==10 ;export_fig test10.png -native
elseif x==11 ;export_fig test11.png -native
elseif x==12 ;export_fig test12.png -native
elseif x==13 ;export_fig test13.png -native
elseif x==14 ;export_fig test14.png -native
elseif x==15 ;export_fig test15.png -native
%
elseif x==16 ;export_fig test16.png -native
elseif x==17 ;export_fig test17.png -native
elseif x==18 ;export_fig test18.png -native
elseif x==19 ;export_fig test19.png -native
elseif x==20 ;export_fig test20.png -native
elseif x==21 ;export_fig test21.png -native
end
% and more...
end;

```

```

imported = cell(1,91);
imported{1,1}=importdata ('test1.png');
imported{1,2}=importdata ('test2.png');
imported{1,3}=importdata ('test3.png');
imported{1,4}=importdata ('test4.png');
imported{1,5}=importdata ('test5.png');
imported{1,6}=importdata ('test6.png');
imported{1,7}=importdata ('test7.png');
imported{1,8}=importdata ('test8.png');
imported{1,9}=importdata ('test9.png');
imported{1,10}=importdata ('test10.png');
imported{1,11}=importdata ('test11.png');
imported{1,12}=importdata ('test12.png');
imported{1,13}=importdata ('test13.png');
imported{1,14}=importdata ('test14.png');
imported{1,15}=importdata ('test15.png');
imported{1,16}=importdata ('test16.png');
imported{1,17}=importdata ('test17.png');
imported{1,18}=importdata ('test18.png');
imported{1,19}=importdata ('test19.png');
imported{1,20}=importdata ('test20.png');
imported{1,21}=importdata ('test21.png');
% and more...
importedgrayR = cell(1,91);
importedbinR = cell(1,91);
for x=[64:91] %1:4 5:14 15:35 22:42 43:59
    imported{1,x}{:,:,2:3} = 0;          %% activate rgb red channel only(from white and
black to red and black)-- non-red using Areas included into black object
% figure,imshow(imported{1,x},'border','tight');
importedgrayR{1,x} = rgb2gray(imported{1,x});
% figure,imshow(importedgrayR{1,x},'border','tight');
importedbinR{1,x} = im2bw(importedgrayR{1,x},.2);

```



```

% figure,imshow(importedbinR{1,x},'border','tight');
end

imported{1,1}=importdata ('test1.png');
imported{1,2}=importdata ('test2.png');
imported{1,3}=importdata ('test3.png');
imported{1,4}=importdata ('test4.png');
imported{1,5}=importdata ('test5.png');
imported{1,6}=importdata ('test6.png');
imported{1,7}=importdata ('test7.png');
imported{1,8}=importdata ('test8.png');
imported{1,9}=importdata ('test9.png');
imported{1,10}=importdata ('test10.png');
imported{1,11}=importdata ('test11.png');
imported{1,12}=importdata ('test12.png');
imported{1,13}=importdata ('test13.png');
imported{1,14}=importdata ('test14.png');
imported{1,15}=importdata ('test15.png');
imported{1,16}=importdata ('test16.png');
imported{1,17}=importdata ('test17.png');
imported{1,18}=importdata ('test18.png');
imported{1,19}=importdata ('test19.png');
imported{1,20}=importdata ('test20.png');
imported{1,21}=importdata ('test21.png');
% and more...
importedgrayB = cell(1,91);
importedbinB = cell(1,91);
for x=[64:91] %1:4 5:14 15:35 1:21 22:42 43:59
imported{1,x}(:,1) = 0; imported{1,x}(:,2) = 0; %% activate rgb blue channel
only(from white and black to blue and black)-- non-blue using Areas included into
black object
% figure,imshow(imported{1,x},'border','tight');
importedgrayB{1,x} = rgb2gray(imported{1,x});

```

```

% figure,imshow(importedgrayB{1,x},'border','tight');
importedbinB{1,x} = im2bw(importedgrayB{1,x},.1);
% figure,imshow(importedbinB{1,x},'border','tight');
end

AfterHough = cell(1,91);
for x=[1:21] %1:4 5:14 15:35 22:42 43:59
AfterHough{1,x}=or(importedbinR{1,x},~importedbinB{1,x});
% figure,imshow(AfterHough{1,x},'border','tight');
end

memberA=cell(1,91);
memberB=cell(1,91);
for x=[64:91] %1:4 5:14 15:35 1:21 22:42 43:59
CC = bwconncomp(~AfterHough{1,x}); %~binary{1,x} and ~AfterHough{1,x}
L = labelmatrix(CC);
s = regionprops(~AfterHough{1,x},
'Area','MajorAxisLength','Perimeter','PixelList','EquivDiameter');%L

%
for k=1:CC.NumObjects
roundness(k)=0;
roundness(k) = 4*(s(k).Area)/pi/((s(k).MajorAxisLength)^2);

end

% area_values = [s.Area];
% idx1 = find (area_values > 550); %550 %'find' determines the indices of array
elements that meet a given logical condition
idx0 = find ( roundness <= .15); %.025 for skeled

% memberB{1,x} = ismember (L,idx0) ;%& ismember(L,idx1) ;
memberA{1,x} = ismember (L,idx0) ;

```

```

[Lm,numm] = bwlabel(member{1,x});
sm = regionprops(Lm, 'Area');
for k=1:numm
    allimg_filarea=allimg_filarea+sm(k).Area;
end

end

mergemem=cell(1,91);
for x=[64:91] %1:4 5:14 15:35 1:21 22:42 43:59
    mergemem{1,x}=or(memberB{1,x},memberA{1,x});
    figure,imshow(~mergemem{1,x},'border','tight');
end

%% GROUNDTRUTHSEGMENT
%% %%//GROUNDTRUTHSEGMENT//%% %%
GT3g = rgb2gray(GT3g);
GT3g = im2bw(GT3g,graythresh(GT3g));
% GT2iigcropped = rgb2gray(GT2iigcropped);
% GT2iigcropped = im2bw(GT2iigcropped,graythresh(GT2iigcropped));
% GT1m = rgb2gray(GT1m);
% GT1m = im2bw(GT1m,graythresh(GT1m));

%% %%Extract Black(Pos-Pos) Only
pairfree=imfuse(~mergememiii{1,55},GT3g); figure,imshow(pairfree,'border','tight');
pairfreegray = rgb2gray(pairfree); figure,imshow(pairfreegray,'border','tight');
CorrectSegmented3gc = im2bw(pairfreegray,.2);
figure,imshow(CorrectSegmented3gc,'border','tight'); %1/2/3/... variable name
change

```

```

pairfree(:,2:3) = 0;          %% activate rgb red channel only(from white and
black to red and black)-- green GT included into black object
pairfreegrayR = rgb2gray(pairfree); %figure,imshow(pairfreegrayR,'border','tight');
CorrectandUnderSeg3gc = im2bw(pairfreegrayR,.2); %
figure,imshow(CorrectandUnderSeg3gc,'border','tight');
UnderSegmented3gc=~xor(CorrectSegmented3gc,CorrectandUnderSeg3gc); %
figure,imshow(UnderSegmented3gc,'border','tight'); %UnderSegmented = green
region
% %
pairfree=imfuse(~mergememiii{1,55},GT3g); %REDOING
pairfree(:,1) = 0; pairfree(:,3) = 0; %% activate rgb green channel only(from
white and black to red and black)--- pink segmented included into black object
pairfreegrayG = rgb2gray(pairfree);
CorrectandOverSeg3gc = im2bw(pairfreegrayG,.2); %
figure,imshow(CorrectandOverSeg3gc,'border','tight');
OverSegmented3gc=~xor(CorrectSegmented3gc,CorrectandOverSeg3gc); %
figure,imshow(OverSegmented3gc,'border','tight'); %OverSegmented = pink
region
%

CC = bwconncomp(~CorrectSegmented3gc); % 2 lines replace bwlabel; -
L = labelmatrix(CC);
ss =regionprops(~CorrectSegmented3gc,'Area');
for k=1:length(ss)
    if k==1; AreaCorrectSegmented3gc=0;
    else
        AreaCorrectSegmented3gc=AreaCorrectSegmented3gc+ss(k).Area;
    end
end
%

CC = bwconncomp(~UnderSegmented3gc); % 2 lines replace bwlabel; -
L = labelmatrix(CC);
ss =regionprops(~UnderSegmented3gc,'Area');

```

```

for k=1:length(ss)
    if k==1; AreaUnderSegmented3gc=0;
    else
        AreaUnderSegmented3gc=AreaUnderSegmented3gc+ss(k).Area;
    end
end
%
CC = bwconncomp(~OverSegmented3gc); % 2 lines replace bwlabel; -
L = labelmatrix(CC);
ss =regionprops(~OverSegmented3gc,'Area');
for k=1:length(ss)
    if k==1; AreaOverSegmented3gc=0;
    else
        AreaOverSegmented3gc=AreaOverSegmented3gc+ss(k).Area;
    end
end
%
%
AreaAllSegments3gc=AreaCorrectSegmented3gc+AreaUnderSegmented3gc+AreaO
verSegmented3gc;

%MorphParValueLabelling
% [Cell,Label]=bwboundaries(~aroped3,'noholes');
%
%
=regionprops(Label,'Area','MajorAxisLength','Perimeter','PixelList','EquivDiameter','
ConvexArea');
% imshow(label2rgb(Label, @jet, [.5 .5 .5]))
% hold on
% numfloc=length(Cell)
% for k=1:length(Cell)
% roundness = 4*(sfl(k).Area)/pi/((sfl(k).MajorAxisLength)^2);
%
% metric_string = sprintf('%2.2f',roundness);

```

```
%  
% boundary = Cell{k}; % obtain (X,Y) boundary coordinates corresponding to  
label 'k'  
% text(boundary(1,2)-35,boundary(1,1)+13,metric_string,'Color','k',...  
% 'FontSize',10,'FontWeight','bold');  
% end
```

